Drainage area, bedrock fracture spacing, and weathering controls on landscape-scale patterns in surface sediment grain size

Alexander. B. Neely[1] and Roman. A. DiBiase[1,2]

[1]Department of Geosciences, Pennsylvania State University, University Park, Pennsylvania, USA 16802

[2]Earth and Environmental Systems Institute, Pennsylvania State University, University Park, Pennsylvania, USA 16802

Corresponding author: Alexander B. Neely (abn5031@psu.edu)

Key Points:

- Surface sediment grain size coarsens ~10-fold downslope in steep, headwater colluvial channels and fines downstream in fluvial channels.
- Surface sediment grain size is tightly coupled to bedrock fracture spacing in steep, rocky catchments.
- Grain size is sensitive to erosion rate in soil-mantled landscapes, but invariant once bedrock hillslopes emerge.

Abstract

Sediment grain size links sediment production, weathering, and fining from fractured bedrock on hillslopes to river incision and landscape relief. Yet, models of sediment grain size delivery to rivers remain unconstrained due to a scarcity of field data. We analyzed how bedrock fracture spacing and hillslope weathering influence landscape-scale patterns in surface sediment grain size across gradients of erosion rate and hillslope bedrock exposure in the San Gabriel Mountains (SGM) and northern San Jacinto Mountains (NSJM) of California, USA. Using ground-based structure-from-motion photogrammetry models of 50 bedrock cliffs, we showed that fracture density is ~5× higher in the SGM than the NSJM. 274 point count surveys of surface sediment grain size measured in the field and from imagery show a drainage area control on sediment grain size, with systematic downslope coarsening on hillslopes and in headwater colluvial channels transitioning to downstream fining in fluvial channels. In contrast to prior work and predictions from a hillslope weathering model, grain size does not increase smoothly with increasing erosion rate. For soil-mantled landscapes, sediment grain size increases with increasing erosion rates; however, once bare bedrock emerges on hillslopes, sediment grain size in both the NSJM and SGM becomes insensitive to further increases in erosion rate and hillslope bedrock exposure, and instead reflects fracture spacing contrasts between the NSJM and SGM. We interpret this threshold behavior to emerge in steep landscapes due to efficient delivery of coarse sediment from bedrock hillslopes to channels and the relative immobility of coarse sediment in fluvial channels.

Plain language Summary

In mountain landscapes, rocks are dislodged from fractured rock to form mobile sediment, and sediment is moved downslope to rivers. Larger sediment requires steeper river slopes to transport, meaning the height of mountain ranges depends on sediment grain size. Sediment is either directly transported to rivers from cliffs or stored on hillslopes as soil where the size of sediment is reduced over time due to weathering. We study how the size of sediment delivered to river channels is affected by (1) bedrock fracture spacing on cliffs and (2) the amount of cliffs relative to the amount of soil on hillslopes. We contrast two landscapes with different bedrock fracture spacing, and we compare bedrock fracture spacing measured on cliffs to the size of sediment in rivers. Also, within each landscape, we compare sediment grain size between steep watersheds with abundant cliffs and watersheds with gentle hillslopes and continuous soil-cover. When bedrock is more fractured, sediment grain size is finer. When hillslopes are gentle and soil-mantled, sediment grain size is reduced on hillslopes, leading to finer river sediment. In steep watersheds with cliffs, sediment moves downslope relatively rapidly, so the grain size of river sediment is large and reflects bedrock fracture spacing.

1. Introduction

As mountain ranges evolve, changes in climate or tectonics affect weathering, soil production, and bedrock fracturing, and these factors also influence hillslope sediment input to rivers (Molnar et al., 2007; Sklar et al., 2017). Thus, in addition to a direct control of climatic and tectonic forcing on landscape evolution, there is a secondary effect via sediment grain size that has network-scale effects on channel geometry, sediment transport, and sediment export to depositional basins (Sklar & Dietrich, 2006; Duller et al., 2010). Channel width and slope must adjust to mobilize the flux and grain size of sediment delivered from hillslopes, meaning fluvial relief in mountain ranges is coupled to sediment production, transport, and grain size fining on hillslopes (Hack, 1957; Sklar & Dietrich, 2006; Johnson et al., 2009). Few field data are available to constrain hillslope controls on network-scale sediment grain size, and this knowledge gap inhibits efforts to understand feedbacks among tectonic and climate forcing, sediment grain size, and topographic relief in mountainous landscapes.

Conceptual frameworks exist to predict the size of sediment delivered to river channels (Sklar et al., 2017), though field data to calibrate and test this framework are generally scarce (e.g. Sklar et al., 2020). In this framework, clasts are produced from fresh bedrock cut by connecting fracture planes, which sets initial sediment grain size (Palmstrom, 2005). As clasts are exhumed, they pass through the near-surface weathering zone on hillslopes where grain size reduction is accomplished by mineral dissolution (e.g., Fletcher & Brantley, 2010) and the generation of new connecting fractures through a variety of processes that may vary depending on climate, biota, mineralogy, and topography (e.g., Riebe et al., 2017). Thus, at the scale of individual hillslopes, the size of sediment delivered to rivers is expected to depend on the initial properties of the inherited bedrock fracture network, the residence time of clasts in the weathering zone, and the rate of chemical and physical weathering processes (Sklar et al., 2017).

Few studies assimilate data that can be used to test controls on landscape-scale patterns in sediment grain size outlined in the above conceptual framework. Detailed measurements of hillslope and channel sediment grain size in the northern California (Attal et al., 2015) and southern Italy (Roda-Boluda et al., 2018) showed that the size of sediment in rivers coarsens as hillslopes steepen, catchment erosion rates increase, and sediment residence time in the weathering zone decreases. Results from these studies inform conceptual models that couple river incision rates and hillslope sediment grain size inputs (Scherler et al., 2017; Shobe et al., 2018). However, these studies do not directly account for: (1) the initial size of clasts set by bedrock fracture spacing; (2) the transition from soil-mantled to bare-bedrock hillslopes; or (3) downstream sorting trends that can complicate comparisons of grain size between different channel-network positions.

Extending analysis of hillslope sediment grain size to steep, rocky landscapes is needed to examine the connection between bedrock fracture spacing and hillslope sediment inputs. By measuring bedrock fracture spacing on bare-bedrock hillslopes, the initial clast size can be more robustly quantified in steep, rocky landscapes than in soil-mantled landscapes (e.g. Moore et al., 2009; Messenzehl et al., 2018; Sklar et al., 2020). Moreover, rocky hillslopes are characteristic of many steep landscapes (DiBiase et al., 2012; Milodowski et al., 2015), and the grain size of sediment supplied from steep rocky hillslopes is a key end-member when describing the range of possible sediment grain sizes supplied to downstream river channels during the lifespan of a mountain range.

Expanding analysis of hillslope sediment grain size inputs to the watershed scale requires an additional incorporation of size-selective sorting and clast-diameter reduction by abrasion that occur as sediment is transported through the sediment routing network (e.g., Brummer & Montgomery, 2003; Attal & Lavé, 2006; Domokos et al., 2014; Miller et al., 2014). Sediment grain size comparisons between separate catchments or landscapes must consider the position of sediment grain size measurements within a drainage network in relation to systematic grain-size sorting trends (e.g. Brummer & Montgomery, 2003). Specifically, we quantify changes in sediment grain size throughout the upland sediment routing network, which progresses downslope from fractured bedrock cliffs, talus, and soil-mantled hillslopes to headwater colluvial (debris flow) channels, fluvial channels, and to catchment outlets on depositional fans. Sampling sediment grain size at this spatial extent and resolution is needed to identify systematic grain size sorting trends, link grain size sorting trends to changes in topographic form, and enable cross-catchment comparisons of sediment grain size that normalize for systematic downslope grain size sorting trends.

In this study, we compare the San Gabriel Mountains and northern San Jacinto Mountains in southern California, where a contrast in bedrock fracture spacing is prevalent on bare-bedrock hillslopes, and sediment residence time in the weathering zone systematically changes as catchment erosion rates increase by 2–3 orders of magnitude in concert with steepening hillslopes and increasing bare-bedrock hillslope abundance (DiBiase et al., 2010; DiBiase et al., 2012; Heimsath et al., 2012; Neely et al., 2019). We use ground-based structure-from-motion photogrammetry to create scaled and georeferenced orthophotos of bedrock cliffs, which enable mapping of the bedrock fracture network and quantification of proxies for initial clast size distributions. We then compare initial clast size distributions from bedrock cliffs to measurements of surface sediment grain size taken from hillslopes and throughout channel networks to quantify systematic grain size sorting patterns at the landscape scale. To analyze weathering controls on sediment grain size, we compare our measurements and published erosion rates to a grain size fining model that depends on bedrock fracture spacing and sediment residence time in the weathering zone. Then, we discuss the role of selective transport and deposition on network-scale patterns in grain size and the implications for interpreting the topography of steep landscapes.

2. Background

2.1 Study area and prior work

We compared bedrock fracture spacing, sediment grain size, and erosion rate throughout watersheds in the San Gabriel Mountains (SGM) and northern San Jacinto Mountains (NSJM) in southern California, USA (Fig. 1). Both landscapes have broadly similar lithology, climate, and vegetation, and each landscape has a robust inventory of detrital in-situ ^{10}Be data that show a spatial pattern in catchment erosion rate that correlates with changes in mean hillslope angle and bare-bedrock exposure on hillslopes (DiBiase et al., 2010; DiBiase et al., 2012; Heimsath et al., 2012; Neely et al., 2019). In both landscapes, erosion rates calculated from ^{10}Be concentrations of cobble (8–12 cm), pebble (2–6 cm), and sand-sized (250–850 μm) fraction samples do not show systematic variations with grain size fraction, differing by a maximum of 38% in the NSJM and a maximum of 35% in the SGM (Neely et al., 2019). Similar ^{10}Be concentrations in detrital samples that range from sand to cobble-sized fractions suggest that erosion rates calculated from sand-sized sediment samples reflect erosion rates across a wider range of grain size classes.

Erosion rates from detrital sands in the SGM range from 0.036 to 2.2 m kyr^{-1} and in the NSJM range from 0.04 to 0.61 m kyr^{-1} (DiBiase et al., 2010; Heimsath et al., 2012; Rossi, 2014; Neely et al., 2019). Hillslopes in both the SGM and NSJM range from fully soil-mantled to ~70% bare-bedrock at the scale of headwater (<7 km^2) catchments, and field observations and soil pits indicate similar soil thicknesses (<1 m) on soil-mantled hillslopes throughout both landscapes (DiBiase et al., 2012; Heimsath et al., 2012; Neely et al., 2019). There is no evidence of Plio-Pleistocene glaciation in either landscape.

The primary difference between the San Gabriel Mountains and northern San Jacinto Mountains is a contrast in bedrock fracture density driven by differences in tectonic setting, which leads to a contrast in initial hillslope grain size inputs between the two landscapes (Fig. 2). DiBiase et al. (2018) used scaled field photographs to measure an approximate 5× contrast in fracture spacing between a single cliff from each landscape, with higher bedrock fracture density in the SGM. In this study, we build on these measurements by quantifying bedrock fracture spacing from structure-from-motion photogrammetry models of 50 bedrock cliffs distributed throughout headwater catchments in the NSJM and SGM.

2.2 Distinction of geomorphic process domains in steep landscapes

Within individual catchments, we define five geomorphic process domains based on morphology and dominant sediment transport process (e.g. Dietrich et al., 2003): (1) bare-bedrock hillslopes; (2) talus and soil-mantled hillslopes; (3) headwater colluvial channels; (4) fluvial channels; and (5) depositional fans (Fig. 3). Steep catchments are typically characterized by a patchwork of soil-mantled and bare-bedrock hillslopes (DiBiase et al., 2012; Neely et al., 2019), along with talus slopes composed of coarse sediment delivered via rockfall and dry ravel from upslope bedrock cliffs. Soil-mantled hillslope and talus-slope morphologies are typically planar and perched near the angle of repose for loose sediment (~35-40 degrees) (e.g. Roering et al., 1999). At the base of hillslopes, headwater colluvial channels form convergent topography in plan-view but have nearly constant down-valley gradients similar to adjacent hillslopes (DiBiase et al., 2012; 2018) (Fig. 3A). Headwater channels are typically mantled in colluvial sediment delivered from surrounding hillslopes, and sediment transport in headwater channel networks is thought to be controlled primarily by mass-wasting and debris flow processes that traverse steep channel gradients (Stock and Dietrich, 2006; Prancevic et al., 2014).

At larger drainage areas in the SGM and NSJM, there is a transition from constant-gradient longitudinal profiles to concave-up longitudinal profiles, which we interpret to reflect fluvial channel heads (Montgomery & Foufoula-Georgiou, 1993; DiBiase et al., 2012; 2018). We assume sediment transport through longitudinally-concave channels is dominated by fluvial processes. Fluvial channels empty into range-front fans where channels are less confined by steep hillslopes, and valley widths widen downstream relative to the width of individual channels. We define fan apexes as the upstream-most elevation of conical fans or back-filled sediment that extents upstream along a constant gradient from conical fan surfaces.

2.3 Prior analysis of hillslopes, headwater channels, and fluvial channels in NSJM and SGM

In the NSJM and SGM, hillslopes remain relatively soil-mantled until mean hillslope angles exceed approximately 35°, consistent with a threshold hillslope stability angle for soil-mantled hillslopes (Carson & Petley, 1970). This hillslope morphology corresponds to erosion rates of 0.08 m kyr^{-1} in the NSJM and 0.2 m kyr^{-1} in the SGM, reflecting more efficient soil

187 production from fractured bedrock in the SGM (Neely et al., 2019). Above mean hillslope angles
188 of 35°, and erosion rates of 0.08 m kyr^{-1} in the NSJM and 0.2 m kyr^{-1} in the SGM, exposure of
189 bare-bedrock hillslopes increases with increasing mean hillslope angle in both landscapes
190 (DiBiase et al., 2012; Neely et al., 2019).

191 Headwater colluvial channels in the SGM and NSJM are typically mantled in sediment
192 and show slopes perched near the angle of repose (33°–35°) (Stock and Dietrich, 2006; DiBiase
193 et al., 2018). Headwater colluvial channels typically form at the base of hillslopes and talus
194 slopes at drainage areas of ~10^3–10^4 m^2 in the SGM and NSJM (DiBiase et al., 2012; Neely et
195 al., 2019). The morphologic transition from constant-gradient headwater-colluvial channels to
196 fluvial channels with characteristic concave-up longitudinal profiles occurs at drainage areas of
197 0.08–0.8 km^2 in the SGM and 0.5–2 km^2 in the NSJM (DiBiase et al., 2012; DiBiase et al.,
198 2018). Headwater colluvial channels have similar gradients in both landscapes, whereas fluvial
199 channels are steeper in the NSJM than the SGM despite having lower catchment averaged
200 erosion rates. The contrast in fluvial steepness between the NSJM and SGM was attributed to
201 wider channels and coarser sediment grain size measured at fan apexes of catchments in the
202 NSJM than at fan apexes of catchments in the SGM (DiBiase et al., 2018).

203 We build on existing sediment grain size data in the NSJM and SGM by systematically
204 measuring sediment grain size throughout the sediment routing network from fractured bedrock
205 to the fan apexes (Fig. 3), and we target catchments that span the full range of erosion rates
206 measured in both landscapes. Existing sediment grain size analyses in the NSJM and SGM
207 (DiBiase et al., 2011; DiBiase et al., 2018) do not consider systematic changes in sediment grain
208 size as a function of position in the sediment routing network (e.g. Brummer & Montgomery,
209 2003; Attal & Lavé, 2006). Additionally, surveys were taken primarily in catchments with steep
210 hillslopes, and do not span the full range of catchment averaged erosion rates observed in both
211 landscapes (DiBiase et al., 2011; DiBiase et al., 2018).

212 ## 3. Methods

213 ### *3.1 Fracture mapping of exposed bedrock cliffs*

214 To constrain initial clast size distributions for each landscape, we measured bedrock
215 fracture density on 50 cliffs in the NSJM (n = 21) and SGM (n = 29) using cliff-normal
216 orthophotos extracted from scaled and georeferenced structure-from-motion photogrammetry
217 models of cliff faces ranging in size from 10^2 to 10^5 m^2 (Fig. 4). Photos were taken from
218 ridgeline camera stations opposite cliffs at distances of 50–1500 m with a Nikon D5500 digital
219 single-lens reflex camera using telephoto lenses (55 and 300 mm focal lengths). The location for
220 each camera station was determined using an EOS Arrow 100 Bluetooth Global Navigation
221 Satellite System (GNSS) receiver (uncertainties typically <5 m). We used Agisoft PhotoScan
222 v1.4.0 (https://www.agisoft.com/) to align GNSS-tagged photographs and construct dense point
223 clouds with an average point spacing of 0.1–1 cm. We refined the alignment of each dense point
224 cloud through iterative closest point alignment to georeferenced airborne lidar point clouds
225 (average point spacing of 10–100 cm) using the software CloudCompare
226 (https://www.cloudcompare.org/) (e.g. Neely et al., 2019). We used the aligned and
227 georeferenced dense point clouds to generate a three-dimensional mesh and then constructed
228 orthophotos from a view perpendicular to the target cliff face, with orthophoto resolutions of 1–3
229 cm (see supplementary dataset).

Bedrock fractures were traced as line features on scaled orthophotos in ESRI ArcMAP v10.6.1 to derive two measures of bedrock fracturing (Fig. 4B). First, we calculated bedrock fracture density (m m^{-2}) as a ratio of the total length of bedrock fracture traces and the area over which bedrock fractures were traced (Dershowitz & Herda, 1992). Second, as a proxy for the initial size distribution of clasts delivered from cliffs, we measured the bedrock fracture spacing, which we define as the apparent short-axis length for each fracture-bound area lying at the intersection of a 2 m grid overlain on the orthophoto (Bunte & Abt, 2001). For bedrock cliffs with sparse fracture spacing (>2 m), grid spacing was increased to 4 m and bedrock fractures were traced over a larger survey area (Table 1). Short-axis lengths between fractures (bedrock fracture spacing) were measured manually using ArcGIS and constrained to be perpendicular to the apparent long-axis, which was identified by eye. These measurements were then compiled to construct a distribution of bedrock fracture spacing values for each cliff face (see supplementary dataset). We assumed that the initial grain size distribution of hillslope clasts in fresh bedrock is set by the bedrock fracture spacing distribution, which may underestimate the intermediate axis of clasts if the short axis is exposed on the cliff face or the orthophoto plane is oriented skew to regional joint sets. To minimize this error, we extracted orthophotos primarily on planar cliff faces perpendicular to joint sets. In contrast, bedrock fracture spacing may overestimate the initial grain size of sediment if clast detachment occurs along finer-scale discontinuities, such as mineral-grain boundaries.

3.2 Sediment grain size distributions on hillslopes and in channels

We used a combination of field point counts, field-based structure-from-motion photogrammetry models of deposits, and aerial-orthophoto surveys to measure surface grain size distributions on hillslopes and throughout channel networks in the SGM and NSJM (Fig. 1). A variety of survey types were required to measure sediment grain size due to accessibility restrictions and the difficulty of measuring coarse (>1 m diameter) grains using tape-measure-based point counts. The resulting 274 grain size surveys have sample sizes of 40–700 individual grains and sample a wide range of hillslope and channel positions (drainage area ranges from 10^2 to 10^7 m^2). Sediment grain size distributions on fans were measured in the active channel near the fan apex.

For field point counts, a 50 m tape measure was laid across the survey reach in 2–6 longitudinal sections spaced 1 m apart in the SGM and 2 m apart in the NSJM, and we measured the intermediate axis of each grain intersected by a meter mark (Wolman, 1954). Field surveys were conducted in summers of 2016, 2017, 2018, and 2019. Surface sediment grain size was measured to millimeter precision in sand and pebble-dominated reaches and centimeter precision in cobble and boulder-dominated reaches.

For field-based structure-from-motion photogrammetry surveys, we photographed deposits from multiple vantage points using either a Nikon D5500 digital single-lens reflex camera with a wide-angle lens (12 mm focal length), an Apple iPhone 4s, or an Apple iPhone 5s. All cameras produced models with point spacing at the millimeter scale because photographs were taken at relatively close range (<10 m). We used Agisoft PhotoScan v1.4.0 to align photographs and generate dense point clouds. Along the edges of each survey region, we included 1–6 scale bars which were used to scale the model and check for distortion, which is typically <2%. For each survey, we generated a high-resolution three-dimensional mesh and 0.1–1 cm resolution orthophoto from a view perpendicular to the deposit surface. Scaled orthophotos

were loaded into ArcMAP 10.6.1 and overlain by a grid with a spacing typically larger than half the width of the largest grain. We measured the apparent short axis of each grain overlain by a grid intersection point using the grid-by-number method (Bunte and Abt, 2001). If the diameter of the intersected grain was buried or obscured by vegetation, the clast diameter was not measured. Large boulders that span multiple intersection points were counted at each grid intersection and for 3 surveys in the SGM, the largest boulders (> 15 m diameter) comprise as much as ~20% of individual survey areas, leading to large D_{84} values in these individual surveys.

In locations with coarser sediment cover, grain size measurements were made continuously on 6–17 cm resolution georeferenced orthophotos from commercial imagery spanning 2011–2017 (Pictometry Corp.; https://www.eagleview.com/product/pictometry-imagery/) (Fig. 5). Similar to the structure-from-motion photogrammetry surveys, we used the grid-by-number method (Bunte & Abt, 2001) to measure the apparent short-axis dimension in planview (assumed to correspond to the intermediate axis) of all clasts in the active channel that intersected a 2 m grid. Clasts overlain by multiple grid intersection points were counted for each grid intersection point. In coarse-grained reaches (D_{50} ~ 2 m), a 4 m grid spacing was used to avoid measuring multiple counts on the majority of clasts in a survey (Fig. 5a), and survey area was increased to measure a comparable number of grains as surveys where a 2 m grid spacing was used. The minimum resolved grain diameter was set to 4 pixels and grid intersections obscured by vegetation or water were not included in the grain size distribution. We defined grain size measurements below the resolving limit (24-68 cm) as "fine" and included these values in the construction of cumulative grain size distributions (e.g. DiBiase et al., 2018). To calculate grain size distributions and facilitate comparison with field-derived data, the continuous channel surveys were broken up into 50–200 m long reaches consisting of 70–400 grains each, depending on tributary junctions and changes in channel width.

To quantify uncertainty in our measurements of median grain size, D_{50}, we performed a bootstrap analysis that considers the full range of measured grain sizes within each landscape at the fluvial channel head position (0.1–1594 cm). We recorded the D_{50} from distributions that contained 1–1000 grains randomly subsampled from full distributions containing 1706 grains in the NSJM and 3981 grains in the SGM. At the 95% confidence interval, D_{50} from subsampled distributions containing 100 individual grains varied by ~30% relative to the D_{50} of the full distribution. This variability reduced to ~15% for subsample sizes containing 500 individual grains, which is typical for amalgamated grain size surveys that consider all surveys taken near ^{10}Be samples and are used to fit model calculations outline in sections below (Table 1).

3.3 Catchment-averaging of fracture density and grain size data

Our analysis focuses on catchments with published catchment averaged erosion rates and bedrock hillslope abundance, and within these catchments, we measured bed sediment grain size and constrained bedrock fracture spacing on representative cliffs. Published catchment averaged erosion rates were tied to catchment outlets of larger catchments (drainage area >7 km^2) and smaller, headwater catchments (drainage areas 0.6–7 km^2). At each ^{10}Be sample location, we compiled nearby fan apex grain size surveys (drainage area >7 km^2) or fluvial channel head grain size surveys (drainage areas 0.05–3 km^2 and 0.5–7 km^2 in the SGM and NSJM respectively). For larger catchments (drainage area >7 km^2), we estimated bedrock hillslope abundance using linear regressions between mean hillslope angle and bedrock hillslope abundance in the NSJM and SGM (Neely et al., 2019) (Table 1).

In all comparisons between sediment grain size and catchment averaged erosion rate, we assume that bed sediment grain size reflects an average bed-state condition over timescales integrated by ^{10}Be-derived erosion rates (10^2–10^6 years). While significant surface grain size variability might be expected at the reach scale over these timescales (e.g. Benda and Dunne, 1997), our analysis compiles 274 individual grain size surveys over regions of >100 km^2 (Fig. 1), and it is unlikely that grain size surveys spanning the spatial scale of our analysis reflect a single, recent large-magnitude event that affected both the NSJM and SGM. In particular, we avoided sampling areas that had been burned within the previous 5 years to avoid bias by fine-grained dry sediment loading (e.g., Lamb et al., 2011).

Within each catchment, bedrock fracture density and bedrock fracture spacing measurements were estimated from sample sizes ranging from 0 to 14 cliffs, due to changes in accessibility and the absence of exposed bedrock cliffs (Table 1). Our ability to resolve local differences in bedrock fracture spacing between watersheds within each landscape is limited; however, the 21–29 cliffs with bedrock fracture measurements in the NSJM and SGM characterize the range of grain size inputs at the scale of each landscape (Fig. 4). We used the summed distribution of all bedrock fracture spacing measurements within each landscape (NSJM or SGM) to determine the distribution of sediment grain size inputs. Although we reported differences in bedrock fracture spacing between individual catchments within each landscape, we assumed that bedrock fracture spacing variability between catchments within each landscape is small compared to larger contrasts in bedrock fracture spacing between the NSJM and SGM (Table 1).

3.4 Hillslope sediment grain size fining model

We compared our measurements of sediment grain size from fluvial channel heads to that predicted from a model of hillslope sediment supply that accounts for changes in bedrock fracture spacing and a time-dependent grain size reduction due to the residence time of clasts within the near surface weathering zone. We compare model results to field data from fluvial channel heads to minimize the effect of systematic downslope grain size sorting, which is not accounted for. Additionally, sediment is coarsest at the fluvial channel head and thus provides a minimum bound on the degree of grain size reduction due to weathering.

We modified a simple model of hillslope grain size reduction used for soil-mantled landscapes (Sklar et al., 2017) to account for the observed transition to bare-bedrock hillslopes that occurs as landscapes steepen and erosion rates increase (DiBiase et al., 2012; Neely et al., 2019). The median grain size of sediment delivered to channels from hillslopes, $D_{50\,channel}$, is modeled according to:

$$\rho D_{50_{modeled}} = \left(1 - f_{bedrock}\right)\left(k_1 D_{50_{fracture}} - k_2 t\right) + f_{bedrock} k_3 D_{50_{fracture}} \qquad (1)$$

where $f_{bedrock}$ is the fraction of bare bedrock in the catchment, $D_{50\,fracture}$ is the D_{50} of bedrock fracture spacing measurements, t is the time spent in the weathering zone, and k_1, k_2, and k_3 are fining constants. Equation 1 represents a linear mixing model where $\left(k¿¿1 D_{50_{fracture}} - k_2 t\right)¿$ is the median grain size of sediment delivered from soil-mantled hillslopes and ¿¿) is the median grain size of sediment delivered from bare-bedrock hillslopes.

We defined $f_{bedrock}$ using a piece-wise function of catchment averaged erosion rate based on field data from the SGM and NSJM:

$$f_{bedrock} = \begin{cases} 0, \wedge for\ E < E_{crit} \\ \alpha\left(E - E_{crit}\right), \wedge for\ E_{crit} < E < E_{maxbr} \\ 1, \wedge for\ E > E_{maxbr} \end{cases} \quad (2a)$$

$$E_{maxbr} = \left(\frac{1}{\alpha}\right) + E_{crit} \quad (2b)$$

where E is the catchment averaged erosion rate, E_{crit} is the erosion rate at which significant bedrock exposure occurs, E_{maxbr} is the erosion rate at which hillslopes become entirely bare bedrock, and α [T L^{-1}] describes how the abundance of bare-bedrock hillslopes increases with increasing erosion rate (Neely et al., 2019). Thus, as erosion rates increase above E_{crit}, the fraction of bare-bedrock hillslopes ($f_{bedrock}$) increases from an initial value of 0, representing a catchment with a continuous soil mantle to a value of 1 at E_{maxbr}, representing a bare-bedrock landscape. Controls on the relationship between $f_{bedrock}$ and catchment erosion rate are still poorly understood, and the physical meaning and variation among different landscapes of the fit parameter α are unclear.

For sediments fined in the weathering zone of soil-mantled hillslopes in the first term of Equation 1, sediment residence time in the weathering zone, t, is defined by:

$$t = h/E \quad (3)$$

where h is thickness of weathering zone (e.g. Attal et al., 2015).

The constants k_1 and k_3 in Equation 1 determine the immediate grain size reduction due to breakage in rockfall or clast detachment along fractures that are below the resolving limit of our fracture spacing measurements (Fig. 6). Because of challenges in measuring initial clast size on soil-mantled hillslopes, we assume this mechanism is the same under soil as on bedrock cliffs ($k_1 = k_3$). k_2 is a rate constant that defines time-dependent mechanisms of grain size reduction (Fig. 6). More specific parameterizations that describe sediment fining on hillslopes as a function of additional environmental variables could be substituted for k_2 (e.g. Sklar et al., 2017; Riebe et al., 2017); however, bedrock fracture spacing appears to be the primary control on the contrast in hillslope erosion and morphology across the SGM and NSJM (Neely et al., 2019), and we assume a constant fining rate in the absence of more specific field constraints.

Because Equation 1 reflects a linear mixing model between sediment supplied from soil-mantled and bare-bedrock hillslopes, additional constraints are needed to describe the morphodynamics of patchy soil-mantled and bare-bedrock hillslopes. For simplicity, we assume that within each catchment soil-mantled and bare-bedrock hillslopes are eroding at the same rate. In the SGM and NSJM, this assumption is supported by similar ^{10}Be concentrations measured in detrital samples taken at the same position but analyzing different grain size fractions (Neely et al., 2019). We also assume that $D_{50\,fracture}$ is the fracture spacing measured on bedrock cliffs, and additional weathering of clasts during transit to channels is accounted for by the value of k_3. For soil mantled hillslopes, we assume for simplicity that the average weathering zone thickness, h, is uniform (Heimsath et al., 2012), and thus, the residence time of sediment in the weathering zone of soil-mantled hillslopes depends only on erosion rate.

To compare the model results to field data, we assumed that $D_{50\,modeled}$ corresponds to the median grain size of fluvial channel head grain size surveys, D_{50}, from headwater catchments where the erosion rate, E, is determined from ^{10}Be concentrations in stream sediments. Although

we focus on the patterns of the D_{50} grain size fraction, similar results may arise from using, for example, the 84th percentile grain size, D_{84}, due to limited variation in sorting across surveys from the SGM and NSJM (Fig. 7). The values of E_{crit} and $D_{50\,fracture}$ for each catchment should depend primarily on rock properties, which show more substantial contrasts between the NSJM and SGM than climatic variables. We assume values of E_{crit} previously calculated for the NSJM and SGM (Neely et al., 2019) and use landscape-averaged values for $D_{50\,fracture}$ in each landscape determined from fracture spacing measurements on 50 cliff-normal orthophotos (Table 2).

We determined the best-fit initial fining coefficient, $k_1=k_3$, and fining-rate coefficient, k_2, by minimizing the sum of the squared residuals in either normalized erosion rate or normalized median grain size. Equation 1 asymptotes at two positions: (1) a minimum erosion rate at which the residence time in the weathering zone leads to sediment fining to a minimum grain size, D_{50min}; and (2) a maximum grain size at high erosion rates, determined by the product of $D_{50\,fracture}$ and k_3 (Fig. 6). Residuals between model fits and field data outside of these bounds become infinite in either grain size or erosion rate, and so we defined a goodness of fit criterion to include residuals in both the normalized median grain size, $D_{50}/D_{50fracture}$, and normalized erosion rate, E/E_{crit} (Fig. 6). We used the minimum of these two residuals, r_i, for each field data point, i, to calculate the sum of the squared residuals, SSR:

$$SSR=\Sigma_i ¿¿, \tag{4a}$$

$$r_i=min\left(\left|\frac{D_{50\,modeled_i}-D_{50i}}{D_{50\,fracture_i}}\right|,\left|\frac{E_{modeled_i}-E_i}{E_{crit_i}}\right|\right). \tag{4b}$$

The values for $k_1=k_3$ and k_2 were determined from a grid-search minimization of *SSR* (Fig. 11, Table 2). A minimum grain size value of D_{50min} = 0.01 cm was chosen because this value is significantly finer than all field measurements, but model fits are insensitive to this boundary condition value.

4. Results

4.1 Bedrock fracture density and bedrock fracture spacing distributions

The mean fracture density of 29 bedrock cliffs in the SGM is 1.8 ± 0.4 (1 standard deviation) m m^{-2}, and the mean fracture density of 20 bedrock cliffs in the NSJM is 0.46 ± 0.12 m m^{-2}. Across SGM cliffs, bedrock fracture density ranges from 0.56 to 4.7 m m^{-2}, whereas bedrock fracture density varies over a smaller range, 0.34–1.2 m m^{-2}, across cliffs in the NSJM (Fig. 4, 8). Combining all bedrock cliffs surveyed, the median bedrock fracture spacing, $D_{50\,fracture}$, is 63 cm in the SGM (3112 measurements) and 299 cm in the NSJM (2344 measurements). For individual cliffs within each landscape, $D_{50\,fracture}$ ranges from 34 to 339 cm in the SGM and from 93 to 482 cm in the NSJM (Fig. 8). There is an inverse relationship between the fracture density and $D_{50\,fracture}$ across all cliffs (Fig. 8). The 5-fold contrast in both bedrock fracture density and bedrock fracture spacing between the NSJM and SGM consistently suggests a 5-fold contrast in initial sediment grain size inputs between both landscapes and is in qualitative agreement with regional observations (DiBiase et al., 2018).

436 *4.2 Surface sediment grain size distributions on hillslopes and in channels*

437 Within both landscapes, sediment grain size varies by ~2-4 orders of magnitude
438 depending on the catchment erosion rate, drainage area, and the grain size distribution statistic
439 analyzed (i.e., D_{16}, D_{50}, D_{84}); however, when isolating these variables, sediment grain size is
440 consistently coarser in NSJM than the SGM (Fig. 9). The D_{50} of all grain size measurements is
441 55 cm in the NSJM and 17 cm in the SGM, and the D_{84} of all grain size measurements is 184 cm
442 in the NSJM and 67 cm in the SGM.

443 In both landscapes, sediment grain size varies by 1-2 orders of magnitude through
444 systematic downslope sorting trends. Sediment grain size coarsens with increasing drainage area
445 along headwater-colluvial channels until reaching fluvial channel heads, where downslope
446 coarsening transitions to downstream fining throughout the fluvial channel network (Fig. 9). The
447 transition from downslope coarsening to downstream fining corresponds to a morphologic
448 transition from steep, constant-gradient headwater-colluvial channels to concave fluvial channels
449 at drainage areas between 0.08 km^2 and 0.8 km^2 in the SGM and 0.5 and 2 km^2 in the NSJM (Fig.
450 9; DiBiase et al., 2018).

451 *4.3 Erosion rate controls on sediment grain size*

452 Between gentle soil-mantled catchments and steep catchments with abundant bare-
453 bedrock hillslopes, there is a contrast in the dependency between catchment erosion rate and
454 stream sediment surface grain size. When catchments are mostly soil-mantled, stream sediment
455 grain size distributions are similar in the SGM and NSJM but coarsen as erosion rates increase in
456 both landscapes, with D_{50} ranging from 0.5 to 6 cm (Fig. 10). In steep, rocky catchments, where
457 $E > E_{crit}$, stream sediment grain size remains relatively constant despite increasing catchment
458 erosion rates; D_{50} at fluvial channel heads is 90–150 cm in the NSJM and 20-40 cm in the SGM,
459 and D_{50} at fans is 29–60 cm in the NSJM and 8–22 cm in the SGM.

460 *4.4 Comparison of field data with predictions from hillslope sediment fining model*

461 In both the NSJM and SGM, the coarsest sediment grain size distributions at fluvial
462 channel heads are approximately half the input grain size distributions estimated from bedrock
463 fracture spacing ($D_{50\,fracture}$), requiring an immediate grain size reduction coefficient, $k_1 = k_3$, of
464 0.4–0.5 (Fig. 11). The values for the best-fit fining rate coefficient, k_2, are 0.05 m kyr^{-1} and 0.025
465 m kyr^{-1} in the NSJM and SGM respectively, which suggests that despite similar bedrock
466 mineralogy and climate, sediment grain size reduction is ~2× faster on hillslopes in the NSJM
467 than the SGM. When erosion rates are rapid and bare-bedrock hillslopes are abundant, changes
468 in catchment-averaged hillslope sediment residence time are small (~ 100–1000 years) relative to
469 best-fit fining rates, and modeled sediment grain size reduction is small (~2-5 cm) relative to the
470 initial D_{50} estimated from bedrock fracture spacing (63-299 cm). Modeled sediment grain size
471 supplied to channels is relatively invariant across a wide range of rapid catchment erosion rates
472 ($E > E_{crit}$), matching field data; however, using the above fining rates, the model does not capture
473 the abrupt coarsening of sediment grain size when erosion rates near E_{crit} in both landscapes.

474 **5. Discussion**

475 Our results show three primary controls on sediment grain size measured at any particular
476 location in a catchment: (1) the initial grain size of sediment set by bedrock fracture spacing; (2)
477 downstream effects due to grain size sorting during sediment transport; and (3) erosion rate as a

proxy for the residence time of sediment in the weathering zone. We discuss how these factors relate to processes that transport sediment through channel networks spanning a range of hillslope morphologies and erosion rates (sections 5.1-5.3), then we examine the implications of systematic grain size trends in the context of landscape evolution over geologic timescales (section 5.4).

5.1 Bedrock fracture spacing and estimating initial sediment grain size

Sediment grain size in the NSJM and SGM mirrors the ~5× contrast in bedrock fracture spacing between these two landscapes. The contrast in fracture spacing is most directly reflected in the grain size of sediment in steep, rocky catchments where sediment residence time in the weathering zone is short, and sediment is effectively transported from bedrock hillslopes to channels. Yet, in steep, rocky catchments, the D_{50} of the coarsest grain size distributions are approximately half as large as the D_{50} of bedrock fracture spacing measured on cliffs (k_3 = 0.4–0.5) (Fig. 11). Contrast between estimated grain size from bedrock fracture spacing and the coarsest D_{50} grain size in channels may reflect sediment sorting, breakage during rockfall or transport, or detachment of sediment along fracture planes that have apertures below the resolution limit of our bedrock-cliff orthophotos (~1 cm resolution) (e.g. Messenzehl et al., 2018). More work is needed to quantify the relative importance of grain detachment along the range of fracture lengths and apertures seen in damaged rock (e.g. Barton & Zobeck et al., 1992; Hooker et al., 2014); however, a similar initial bedrock fining factor (k_3 = 0.4–0.5) determined for landscapes with a large contrast in fracture density suggests a similar grain size reduction mechanism in both landscapes and that our bedrock fracture measurements quantify a similar range of fracture geometries relevant for sediment detachment in the NSJM and SGM.

In contrast to steep, rocky catchments, sediment grain size in soil-mantled catchments is relatively similar between the NSJM and SGM. Similar sediment grain size but sparser bedrock fracture spacing in the NSJM than the SGM requires faster apparent grain size fining rates in the NSJM than the SGM. Bedrock mineralogy and climatic differences are minimal between these mountain ranges, and thus, the drivers of faster apparent grain size fining rates in the NSJM are not immediately obvious. Potentially, more sediment on soil-mantled hillslopes is sourced from grussification along mineral-scale discontinuities rather than detachment along macro-scale fractures. Additionally, boulders detached along fracture planes may be relatively immobile across lower-gradient hillslopes and weather as exhumed corestones during downslope transport (e.g. Fletcher & Brantley, 2010; Glade et al., 2017). Selective transport of fine-grained sediment across low-gradient hillslopes and detachment of sediment by grussification may decouple sediment grain size from bedrock fracture spacing where hillslope gradients are low, a continuous soil mantle exists, and rock is efficiently weathered.

The grain size distribution of sediment in talus piles has been used as a proxy for the grain size distribution of sediment contributed from bedrock cliffs (Attal et al., 2015; Roda-Boluda et al., 2018); however, in the NSJM and SGM, the grain size of sediment in talus piles is much finer (5–10×) than the grain size estimated from bedrock fracture spacing on cliffs (Fig. 9). On individual talus piles, clast travel distances are sensitive to talus pile slope, clast momentum following rockfall height, and the grain size of the mobile clast relative to the roughness of the talus-slope surface (Kirkby & Statham, 1975; DiBiase et al., 2017). In the NSJM and SGM, the coarsest grains supplied from bedrock cliffs bypass steep talus slopes with small upstream drainage areas (< ~0.01 km^2) and are located at the base of headwater colluvial channels,

meaning that the coarsest grain size fraction is not captured by the grain size distribution of sediment on individual talus slopes adjacent to source cliffs (Fig. 9). Because grain size sorting occurs immediately after clasts are dislodged from intact bedrock, bedrock fracture spacing on cliffs serves as a more direct measure of the initial sediment grain size; however, more work is needed to describe controls on k_3, which describes the relationship between sediment grain size, the range of fracture lengths and apertures in a rock mass, and processes that detach clasts along fractures of different geometry (e.g. Sklar et al., 2017).

5.2 Drainage area dependent patterns in sediment grain size within each landscape

In the NSJM and SGM, downslope and downstream sorting are observed at the scale of individual talus slopes and at the scale of entire watersheds, suggesting that sorting associated with sediment transport is a first order control on sediment grain size. On steep talus slopes (drainage area < ~0.01 km^2), downslope coarsening trends are consistent with results from rockfall and talus slope models and experiments (e.g., Rapp, 1960; Kirkby & Statham, 1975). Observed downslope coarsening trends are inconsistent with progressive weathering as particles move down slope, which would generate downslope fining after sediment is detached from cliffs (Glade et al., 2017) and may have a stronger expression in catchments with gentler hillslopes and slower hillslope erosion rates.

In steep catchments, sediment grain size continues to coarsen downslope throughout the headwater-colluvial channel network. We hypothesize that this pattern primarily results from debris flow transport of coarse-grained sediment towards the base of headwater colluvial channels, where decreases in slope often coincide with tributary junctions (Stock & Dietrich, 2006). Repeated deposition of coarse-grained debris flow snouts may concentrate coarse-grained sediment at the base of steep, headwater channels and the upstream extent of the fluvial channel network (Fig. 9). The transition from downslope coarsening in headwater colluvial channels to downstream fining in fluvial channels is consistent with a transition in dominant sediment transport process at drainage areas of 0.08–2 km^2 in SGM and NSJM (DiBiase et al., 2012; DiBiase et al., 2018), and is broadly similar to observations of downslope coarsening in headwater channels of western Washington interpreted to result from debris flow transport (Brummer and Montgomery, 2003).

Fining throughout the fluvial network could be driven by selective transport, abrasion, or downstream changes in hillslope sediment grain size inputs (e.g., Pizzuto, 1995; Attal and Lavé 2006; Menting et al., 2015). In both the NSJM and SGM, hillslope gradients and erosion rates do not systematically change downstream (Neely et al., 2019), suggesting that downstream changes in hillslope sediment grain size inputs are unlikely to drive consistent downstream fining trends (e.g., Lukens et al., 2016; Sklar et al., 2020). Given typical abrasion rates for granitic bedrock, abrasion is unlikely to fine sediment by 50–75% over transport distances of ~10 km (Attal & Lavé, 2009). We suggest that size-selective transport is the primary factor that controls downstream fining trends over these small watersheds the NSJM and SGM; however, downstream measurements of boulder shape could potentially be used to distinguish between size-selective transport and abrasion controls on downstream fining (e.g. Miller et al., 2014).

Size-selective transport in NSJM and SGM channels may result from large clast sizes relative to channel width and flow depth, which promotes grain protrusion from flows and formation of reach-spanning boulder-jams. These factors preferentially increase the stability of coarse-grained sediment in steep, narrow channels with low flow depths, such that fine-grained

sediment is winnowed downstream (e.g., Lamb et al., 2008; Zimmerman et al., 2010; Attal et al., 2017). At larger drainage areas, fluvial channels progressively widen and deepen relative to maximum clast sizes, and the relative mobility across all grain size classes may be more uniform, leading to systematic downstream fining trends.

5.3 Erosion rate and bedrock exposure controls on sediment grain size distributions

In both landscapes, slowly eroding soil-mantled catchments have finer surface-sediment grain size than catchments with steep, rapidly eroding threshold hillslopes with abundant bare-bedrock cliffs, indicating a residence-time dependence on stream-sediment grain size. Sediment residence time in the weathering zone decreases with increasing erosion rate due to both more rapid erosion and effective thinning of the weathering zone due to increased bedrock exposure. Although the thickness of soil on soil-mantled hillslopes does not decrease considerably with increasing erosion rate in these landscapes (Heimsath et al., 2012), the abundance of bare bedrock cliffs increases (Neely et al., 2019), which reduces the effective weathering zone thickness at the catchment-scale.

The grain size of sediment at fluvial channel heads does not show smoothly coarsening D_{50} grain size with decreasing sediment residence time in the weathering zone; instead, there is a dichotomy between sediment grain size in catchments with gentle, soil-mantled hillslopes and catchments with steep hillslopes and bare-bedrock cliffs (Fig. 11). A linear relationship between grain size fining and erosion rate (Eq. 1) can generally reproduce the observed stream grain sizes using fining rates that are consistent with typical weathering rates of bedrock tors in granitic landscapes (k_2 = 0.025–0.05 m kyr^{-1}) (Portenga & Bierman, 2011). Yet, this model may be misleading if: (1) a different proportion of clasts are detached along fracture planes and mineral-scale discontinuities as a function of changing erosion rate and sediment residence time in the weathering zone (i.e. an erosion rate control on k_3); or (2) if sediment is selectively transported through the river network such that grain size inputs supplied from hillslopes do not reflect the grain size of surface sediment cover at fluvial channel heads. Our channel grain size measurements indicate that erosion rates primarily control bed sediment grain size through E_{crit}, the erosion rate at which hillslopes transition from gentle, soil-mantled morphologies to steep hillslopes with increasing abundance of bare-bedrock cliffs.

In contrast to the hillslope sediment fining model (Eq. 1), we interpret the sediment grain size dichotomy between gentle, soil-mantled and steep, rocky catchments to reflect a transition where bedrock exposure on steep hillslopes is a threshold that initiates delivery of coarse sediment from rockfall, landslides, and debris flows (e.g. Roda-Boluda et al., 2018). Because of the relative immobility of the coarsest grain size fraction in steep, narrow channels (e.g. Rickenmann, 2001), sediment supply from even a small amount of bedrock cliffs mantles channels with coarse sediment that directly reflects bedrock fracture spacing. Channel response to coarse sediment inputs (e.g. Shobe et al., 2016) winnows finer sediment supplied from hillslopes downstream to depositional fans, leading to observed downstream fining trends (Fig. 9; Fig. 12). Although the grain size of the sediment flux exiting watersheds is likely sensitive to decreasing soil cover on hillslopes, changing the abundance of soil-mantled and bare-bedrock hillslopes as erosion rates exceed E_{crit} has minimal effect on the grain size of bed surface cover in NSJM and SGM channels, because the grain size of stream bed sediment more strongly reflects the coarse sediment fraction delivered from exposed bedrock cliffs (Fig. 12B-C). If channel morphology is set in part by an initiation of motion threshold that depends on the grain size of

surface cover (Lague et al., 2005; DiBiase & Whipple, 2011; Phillips & Jerolmack, 2016), fracture density emerges as a direct control on sediment grain size and an indirect control on the morphology of rivers across a potentially wide range of hillslope erosion rates that exceed E_{crit}.

5.4 Implications of systematic grain size trends for landscape evolution over geologic timescales

At the watershed scale, changes in sediment grain size observed within and between the NSJM and SGM have implications for interpreting channel morphodynamics in headwater-colluvial and fluvial channels. Within the NSJM and SGM, downslope coarsening trends are consistent with downstream increases in unit stream power along steep, constant-gradient headwater-colluvial channels (e.g. Brummer and Montgomery, 2003); however, comparing the NSJM and SGM, headwater channels show similar channel gradients of 33-35°, despite ~5× coarser sediment grain size in the NSJM than the SGM (DiBiase et al., 2018). Steep, headwater channel morphodynamics appear relatively insensitive to sediment grain size contrasts between these two landscapes, which is consistent with an interpretation that mass-wasting processes dominate sediment transport across channel reaches with gradients that approach frictional stability limits for loose sediment (Prancevic et al., 2014). In contrast, fluvial channel gradients are steeper in the NSJM than the SGM, reflecting grain size differences between these landscapes and confirming prior interpretations that sediment grain size controls fluvial channel steepness in these landscapes (DiBiase et al., 2018). It remains less clear how observed downstream patterns in grain size impact the drainage density and concavity of headwater and fluvial channel networks (e.g. Gasparini et al., 2004).

At the landscape scale, our results imply a strong connection among bedrock fracturing, sediment grain size, and the efficiency of river incision in steep mountain ranges (Molnar et al., 2007; Johnson et al, 2009; DiBiase et al., 2018). Our results show that in steep landscapes, surface sediment grain size reflects coarse sediment inputs from bedrock cliffs and landslides, whereas the total flux of sediment likely includes a larger fraction of fine-grained sediment sourced from soil-mantled hillslopes and mineral-scale grussification (Fig. 12). Conceptual models that predict continuously coarsening hillslope sediment supply with increasing catchment erosion rate may accurately reflect grain size changes in the total sediment flux (Scherler et al., 2017; Sklar et al., 2017; Shobe et al., 2018); however, bed sediment grain size responsible for setting channel geometry appears insensitive to increases in catchment erosion rate once erosion rates exceed E_{crit}. When erosion rates exceed E_{crit}, coarse sediment is supplied from bedrock cliffs and landslides, and this coarser, less-mobile grain size fraction preferentially mantles channel beds, even if these coarse-grained sediment sources contribute only a relatively small portion of the total sediment flux (Fig. 11; Fig. 12). Constant bed sediment grain size across a wide range of erosion rates exceeding E_{crit} in the NSJM and SGM, implies a weak feedback between time-dependent weathering processes, sediment grain size delivered to rivers, and channel morphology. Instead, bedrock fracture spacing emerges as a primary control on bed sediment grain size in steep, rocky landscapes across a wide range of erosion rates that exceed E_{crit}.

Although weathering controls on bed sediment grain size appear minimal in steep mountain ranges where catchment erosion rates exceed E_{crit}, E_{crit} reflects the efficiency of soil transport and soil production within a landscape and varies over at least two orders of magnitude globally as a function of climate, lithology, and bedrock fracture spacing (Neely et al., 2019). Thus, changes in climate, lithology, or bedrock fracture spacing can additionally affect the grain

size of bed sediment in rivers by changing E_{crit}, the catchment erosion rate below which sediment grain size fines as a function of residence time on gentle, soil-mantled hillslopes.

In landscapes where soil is efficiently produced from fresh bedrock and transported downslope, gentle, continuously soil-mantled hillslopes can persist at more rapid channel incision rates, and bed sediment grain size may be more strongly influenced by hillslope weathering rather than bedrock fracture spacing. In the NSJM and SGM, bed sediment grain size coarsens approximately 1-2 orders of magnitude between catchments with soil-mantled hillslopes and erosion rates below E_{crit} and catchments with steep, rocky hillslopes and erosion rates above E_{crit} (Fig. 10). Changes in E_{crit} due to changes in climate or rock strength not only affect the amount of soil cover in upland landscapes for a given hillslope erosion rate (e.g. Neely et al., 2019), but also can affect the efficiency of river incision and the overall relief of mountain landscapes by changing the grain size of sediment mantling stream channels for a given hillslope erosion rate.

6. Conclusions

Our analysis from the NSJM and SGM shows that surface sediment grain size is primarily affected by three factors: (1) inherited bedrock fracture spacing, which controls the initial grain size of sediment delivered from hillslopes to channels; (2) grain size sorting during sediment transport processes that operate on hillslopes and in colluvial and fluvial channels; and (3) catchment erosion rate, which controls the abundance of bare-bedrock hillslopes and the residence time of sediment in the weathering zone. Surface sediment grain size is coarser in the NSJM than in the SGM, reflecting the contrast in bedrock fracture spacing measured on cliffs. The connection between fracture spacing and grain size is strongest in catchments where erosion rates exceed E_{crit} and bare bedrock hillslopes are exposed. In contrast to prior conceptual models, once bedrock hillslopes emerge, surface sediment grain size appears to be insensitive to further increases in erosion rates and hillslope bedrock exposure.

In both landscapes, surface sediment grain size of talus deposits is much finer (5–10×) than the grain size estimated from bedrock fracture spacing on cliffs. Surface sediment grain size coarsens downslope throughout talus deposits and steep, headwater colluvial channels, and bed sediment grain size fines downstream throughout fluvial channels at larger drainage areas. The transition from downslope coarsening to downstream fining at fluvial channel heads is consistent with a change in dominant sediment transport process at this location, from mass-wasting in headwater channels to fluvial entrainment downstream.

Comparison between bed-sediment grain size and catchment erosion rates suggests that emergence of bedrock cliffs on steep hillslopes fundamentally changes the bed-state of river channels. Coarse sediment delivered from fractured bedrock cliffs and headwater colluvial channels accumulates in steep fluvial channels, and finer sediment is winnowed downstream. This result is supported by observed downstream fining trends in the fluvial networks of the NSJM and SGM and contradicts conceptual models that predict continuously coarsening bed sediment grain size with increasing catchment erosion rate and bare-bedrock hillslope abundance. Instead, this result implies strong feedbacks between bedrock fracturing, bed sediment grain size, and the efficiency of river incision in steep mountain ranges, whereby the transition from soil-mantled to bedrock hillslopes indicates a change from weathering-dependent to bedrock fracture spacing dependent controls on the grain size of sediment mantling river channels.

Acknowledgments

Project supported by National Science Foundation grant EAR-1608014 to R. DiBiase. Low-altitude aerial imagery was acquired by Pictometry Corporation. Airborne lidar-derived topographic data was acquired by National Center for Airborne Laser Mapping. 3-D point clouds and digital orthophotos are available through *OpenTopography.org*. Data tables containing bedrock fracture spacing measurements and stream grain size measurements are provided as supplementary tables and GIS shapefiles. We acknowledge Angeles National Forest, San Bernardino National Forest, and Mt. San Jacinto State Park for continued trail maintenance enabling access to field sites. We thank J. Carr, J. Del Vecchio, E. Greenberg, and P. Silverhart for field assistance, E. Loucks for assistance constructing structure-from-motion models, and McLanahan's downtown market for providing a comfortable workspace during the preparation of this manuscript. We thank Mikael Attal, Claire Lukens, and one anonymous reviewer for their thoughtful reviews and suggestions that improved the clarity of this manuscript.

References

Attal, M, & Lavé, J. (2006). Changes of bedload characteristics along the Marsyandi River (central Nepal): Implications for understanding hillslope sediment supply, sediment load evolution along fl uvial networks, and denudation in active orogenic belts. in *Tectonics, Climate, and Landscape Evolution*, Willett, S. D., Hovius, N, Brandon, M. T., & Fisher, D. (eds). *Geological Society of America Special Paper*, 398, 143–171. https://doi.org/10.1130/2006.2398(09).

Attal, M, & Lavé, J. (2009). Pebble abrasion during fluvial transport: experimental results and implications for the evolution of the sediment load along rivers. *Journal of Geophysical Research*, *114*, F04023. https://doi.org/10.1029/2009JF001328

Attal, M., S. M. Mudd, M. D. Hurst, B. Weinman, K. Yoo, & M. Naylor (2015). Impact of change in erosion rate and landscape steepness on hillslope and fluvial sediments grain size in the Feather River basin (Sierra Nevada, California), *Earth Surface Dynamics*, *3*, 201–222. https://doi.org/10.5194/esurf-3-201-2015

Attal, M. (2017). Linkage Between Sediment Transport and Supply in Mountain Rivers. In Gravel−Bed Rivers (eds D. Tsutsumi and J.B. Laronne). doi:10.1002/9781118971437.ch12

Barton, C. A., & Zoback, M. D. (1992). Self−similar distribution and properties of macroscopic fractures at depth in crystalline rock in the Cajon Pass Scientific Drill Hole, *Journal of Geophysical Research*, *97(B4)*, 5181–5200, https://doi.org/10.1029/91JB01674.

Benda, L., & Dunne, T. (1997). Stochastic forcing of sediment routing and storage in channel networks, *Water Resources Research*, *33(12)*, 2865–2880, doi:10.1029/97WR02387.

Brummer, C. J., & Montgomery, D. R. (2003). Downstream coarsening in headwater channels. *Water Resources Research*, *39(10)*, 1294. https://doi.org/10.1029/2003WR001981

Bunte, K., & Abt, S. R. (2001). Sampling surface and subsurface particle−size distributions in wadable gravel− and cobble−bed streams for analyses in sediment transport, hydraulics, and Streambed monitoring (General Tech. Rep. RMRS−GTR−74). Fort Collins, CO: US Department of Agriculture, Forest Service, Rocky Mountain Research Station.

738 Carson, M. A., & Petley, D. J. (1970). The existence of threshold slopes in the denudation of the
739 landscape, *Transactions of the Institute of British Geographers*, *49*, 71–95.
740 https://doi.org/10.2307/621642

741 Dershowitz, W. S., & Herda, H. H. (1992). Interpretation of fracture spacing and intensity, Proc.
742 U.S. Rock Mech. Symp. 33rd, 10.

743 Dietrich, W.E., Bellugi, D.G., Sklar, L.S., Stock, J.D., Heimsath, A.M. & Roering, J.J., (2003).
744 Geomorphic transport laws for predicting landscape form and dynamics. *Geophysical*
745 *Monograph-American Geophysical Union*, 135, pp.103-132.
746 https://doi.org/10.1029/135GM09

747 DiBiase, R. A., Whipple, K. X., Heimsath, A. M., & Ouimet, W. B. (2010). Landscape form and
748 millennial erosion rates in the San Gabriel Mountains, CA, *Earth and Planetary Science*
749 *Letters*, *289(1–2)*, 134–144, https://doi.org/10.1016/j.epsl.2009.10.036.

750 DiBiase, R. A., & Whipple, K. X. (2011). The influence of erosion thresholds and runoff
751 variability on the relationships among topography, climate, and erosion rate, *Journal of*
752 *Geophysical Research: Earth Surface*, *116*, F04036,
753 https://doi.org/10.1029/2011JF002095.

754 DiBiase, R.A., Heimsath, A.M., & Whipple, K.X. (2012). Hillslope response to tectonic forcing
755 in threshold landscapes. *Earth Surface Processes and Landforms*, *37(8)*, 855–865. https://
756 doi.org/10.1002/esp.3205

757 DiBiase, R.A., Lamb, M.P., Ganti, V. & Booth, A.M. (2017). Slope, grain size, and roughness
758 controls on dry sediment transport and storage on steep hillslopes. *Journal of*
759 *Geophysical Research: Earth Surface*, *122(4)*, 941–960.
760 https://doi.org/10.1002/2016JF003970

761 DiBiase, R.A., Rossi, M.W. & Neely, A.B. (2018). Fracture density and grain size controls on
762 the relief structure of bedrock landscapes. *Geology*, *46(5)*, 399–402.
763 https://doi.org/10.1130/G40006.1

764 Domokos, G., Jerolmack, D.J., Sipos, A.Á. & Török, Á., (2014). How river rocks round:
765 resolving the shape-size paradox. *PloS one*, 9(2).
766 https://doi.org/10.1371/journal.pone.0088657

767 Duller, R.A., Whittaker, A.C., Fedele, J.J., Whitchurch, A.L., Springett, J., Smithells, R.,
768 Fordyce, S. & Allen, P.A. (2010). From grain size to tectonics. *Journal of Geophysical*
769 *Research: Earth Surface*, *115*(F3). https://doi.org/10.1029/2009JF001495

770 Fletcher, R.C., & Brantley, S.L. (2010). Reduction of bedrock blocks as corestones in the
771 weathering profile: observations and model. *American Journal of Science*, *310(3)*, 131–
772 164. https://doi.org/10.2475/03.2010.01

773 Gasparini, N. M., Tucker, G. E., & Bras, R. L. (2004). Network‐scale dynamics of grain‐size
774 sorting: Implications for downstream fining, stream‐profile concavity, and drainage
775 basin morphology. Earth Surface Processes and Landforms, 29(4), 401-421.
776 https://doi.org/10.1002/esp.1031

Glade, R.C., Anderson, R.S., & Tucker, G.E. (2017). Block-controlled hillslope form and persistence of topography in rocky landscapes. *Geology*, *45(4)*, 311–314. https://doi.org/10.1130/G38665.1

Hack, J. T. (1957). Studies of longitudinal stream profiles in Virginia and Maryland, U.S. Geol. Surv. Prof. Pap., 294−B, 97.

Heimsath, A. M., DiBiase, R. A., & Whipple, K. X. (2012). Soil production limits and the transition to bedrock−dominated landscapes, *Nature Geoscience*, *5*, 210–214, https://doi.org/10.1038/NGEO1380.

Hooker, J. N., Laubach, S. E., & Marrett, R. (2014). A universal power−law scaling exponent for fracture apertures in sandstones, *GSA Bulletin*, *126(9−10)*, 1340–1362, https://doi.org/10.1130/B30945.1.

Jennings, C.W., Strand, R.G., & Rogers, T.H. (1977). Geologic map of California: California Division of Mines and Geology, scale 1:750,000

Johnson, J.PL., Whipple, K.X., Sklar, L.S., & Hanks, T.C. (2009). Transport slopes, sediment cover, and bedrock channel incision in the Henry Mountains, Utah. *Journal of Geophysical Research* 114, F02014. DOI:10.1029/2007JF000862.

Kirkby, M.J. & Statham, I. (1975). Surface stone movement and scree formation. *The Journal of Geology*, *83(3)*, 349–362. https://doi.org/10.2307/30059027

Lague, D., Hovius, N. & Davy, P. (2005). Discharge, discharge variability, and the bedrock channel profile. *Journal of Geophysical Research: Earth Surface*, *110,* F4, https://doi.org/10.1029/2004JF000259

Lamb, M. P., Dietrich, W. E., & Venditti, J. G. (2008). Is the critical Shields stress for incipient sediment motion dependent on channel−bed slope? *Journal of Geophysical Research: Earth Surface*, *113*, F02008, https://doi.org/10.1029/2007JF000831

Lamb, M. P., Scheingross, J. S., Amidon, W. H., Swanson, E., & Limaye, A. (2011). A model for fire−induced sediment yield by dry ravel in steep landscapes, *Journal of Geophysical Research: Earth Surface*, *116*, F03006, https://doi.org/10.1029/2010JF001878

Lukens, C.E., Riebe, C.S., Sklar, L.S. & Shuster, D.L., (2016). Grain size bias in cosmogenic nuclide studies of stream sediment in steep terrain. *Journal of Geophysical Research: Earth Surface*, 121(5), pp.978-999. https://doi.org/10.1002/2016JF003859

Menting, F., Langston, A. L., & Temme, A. J. A. M. (2015). Downstream fining, selective transport, and hillslope influence on channel bed sediment in mountain streams, Colorado Front Range, USA. *Geomorphology*, *239*, 91–105. https://doi.org/10.1016/j.geomorph.2015.03.018

Messenzehl, K., Viles, H., Otto, J.−C., Ewald, A., & Dikau, R. (2018). Linking rock weathering, rockwall instability and rockfall supply on talus slopes in glaciated hanging valleys (Swiss Alps). *Permafrost and Periglacial Processes*, *29*, 135–151. https://doi.org/10.1002/ppp.1976

Milodowski, D. T., Mudd, S. M., & Mitchard, E. T. A. (2015). Topographic roughness as a signature of the emergence of bedrock in eroding landscapes, *Earth Surface Dynamics*, *3(4)*, 483–499, https://doi.org/10.5194/esurf-3-483-2015

Molnar, P., Anderson, R. S., & Anderson, S. P. (2007). Tectonics, fracturing of rock, and erosion, *Journal of Geophysical Research: Earth Surface*, *112*, F03014, https://doi.org/10.1029/2005JF000433

Montgomery, D. R., & Foufoula‐Georgiou, E. (1993). Channel network representation using digital elevation models, *Water Resources Research*, *29*, 1178–1191. https://doi.org/10.1029/93WR02463

Moore, J. R., Sanders, J. W., Dietrich, W. E., & Glaser, S. D. (2009). Influence of rock mass strength on the erosion rate of alpine cliffs, *Earth Surface Processes and Landforms*, *34*, 1339–1352, https://doi.org/10.1002/esp.1821

Neely, A. B., DiBiase, R. A., Corbett, L. B., Bierman, P. R., & Caffee, M.W. (2019). Bedrock fracture density controls on hillslope erodibility in steep, rocky landscapes with patchy soil cover, southern California, USA. *Earth and Planetary Science Letters*, *522*, 186–197. https://doi.org/10.1016/j.epsl.2019.06.011

Palmstrom, A. (2005). Measurements of and correlations between block size and rock quality designation (RQD). *Tunnelling and Underground Space Technology*, *20(4)*, 362–377. https://doi.org/10.1016/j.tust.2005.01.005

Phillips, C. B., & Jerolmack, D. J. (2016). Self‐organization of river channels as a critical filter on climate signals, *Science*, *352(6286)*, 694–697, https://doi.org/10.1126/science.aad3348

Pizzuto, J.E. (1995). Downstream fining in a network of gravel‐bedded rivers. *Water Resources Research*, *31(3)*, 753–759. https://doi.org/10.1029/94WR02532

Portenga, E. W., & Bierman, P. R. (2011). Understanding Earth's eroding surface with ^{10}Be. *GSA today*, *21(8)*, 4–10. http://dx.doi.org/10.1130/G111A.1

Prancevic, J. P., Lamb, M. P., & Fuller, B. M. (2014). Incipient sediment motion across the river to debris-flow transition. *Geology*, *42(3)*, 191–194. https://doi.org/10.1130/G34927.1

Rapp, A. (1960). Recent development of mountain slopes in Karkevagge and surroundings, northern Scandinavia, *Geografiska Annaler*, *42*, 65–200, https://doi.org/10.2307/520126

Rickenmann, D. (2001). Comparison of bed load transport in torrents and gravel bed streams. *Water Resources Research*, *37(12)*, 3295–3305. https://doi.org/10.1029/2001WR000319

Riebe, C. S., Hahm, W. J., & Brantley, S. L. (2017). Controls on deep critical zone architecture: A historical review and four testable hypotheses. *Earth Surface Processes and Landforms*, *42(1)*, 128–156. https://doi.org/10.1002/esp.4052

Roda-Boluda, D. C., D'Arcy, M., McDonald, J., & Whittaker, A. C. (2018). Lithological controls on hillslope sediment supply: Insights from landslide activity and grain size distributions. *Earth Surface Processes and Landforms*, *43(5)*, 956–977. https://doi.org/10.1002/esp.4281

Roering, J.J., Kirchner, J.W., & Dietrich, W.E., (1999). Evidence for nonlinear, diffusive sediment transport on hillslopes and implications for landscape morphology. *Water Resouces. Res*earch 35 (3), 853–870. https://doi.org/10.1029/1998WR900090.

Rossi, M. W. (2014), Hydroclimatic Controls on Erosional Efficiency in Mountain Landscapes [Ph.D. Thesis]: Tempe, Arizona, Arizona State University.

Scherler, D., DiBiase, R. A., Fisher, G. B., & Avouac, J.−P. (2017). Testing monsoonal controls on bedrock river incision in the Himalaya and Eastern Tibet with a stochastic−threshold stream power model. *Journal of Geophysical Research: Earth Surface*, *122*, 1389–1429. https://doi.org/10.1002/2016JF004011

Shobe, C. M., Tucker, G. E., & Anderson, R. S. (2016). Hillslope−derived blocks retard river incision. *Geophysical Research Letters*, *43*, 5070–5078. https://doi.org/10.1002/2016GL069262

Shobe, C. M., Tucker, G. E. & Rossi, M. W. (2018). Variable−threshold behavior in rivers arising from hillslope−derived blocks. *Journal of Geophysical Research: Earth Surface*, *123*(8), 1931–1957. https://doi.org/10.1029/2017JF004575

Sklar, L. S., & Dietrich, W. E. (2006). The role of sediment in controlling steady−state bedrock channel slope: Implications of the saltation−abrasion model. *Geomorphology*, *82(1–2)*, 58–83. https://doi.org/10.1016/j.geomorph.2005.08.019

Sklar, L. S., Riebe, C. S., Marshall, J. A., Genetti, J., Leclere, S., Lukens, C. L., & Merces, V. (2017). The problem of predicting the size distribution of sediment supplied by hillslopes to rivers. *Geomorphology*, *277*, 31–49. https://doi.org/10.1016/j.geomorph.2016.05.005

Sklar, L.S., Riebe, C.S., Genetti, J., Leclere, S. & Lukens, C.E., (2020). Downvalley fining of hillslope sediment in an alpine catchment: implications for downstream fining of sediment flux in mountain rivers. *Earth Surface Processes and Landforms*. https://doi.org/10.1002/esp.4849

Stock, J. D., & Dietrich, W. E. (2006), Erosion of steepland valleys by debris flows, *GSA Bulletin*, *118*, 1125–1148, https://doi.org/10.1130/B25902.1

Wolman, M. G. (1954). A method of sampling coarse river−bed material. *Eos, Transactions of the American Geophysical Union*, *35(6)*, 951–956. https://doi.org/10.1029/TR035i006p00951

Zimmermann, A., Church, M. & Hassan, M. A. (2010). Step−pool stability: Testing the jammed state hypothesis. *Journal of Geophysical Research: Earth Surface*, *115(F2)*. https://doi.org/10.1029/2009JF001365

888 **Table 1.** Surface sediment grain size and catchment attributes at fluvial channel head and fan
889 apex ^{10}Be sample locations for catchments in the San Gabriel Mountains (SGM, SG sample
890 numbers) and the northern San Jacinto Mountains (NSJM, SJ sample numbers).

891

SGM [1]Fans	Drainage area (km^2)	Outlet Latitude (°)	Outlet Longitude (°)	Erosion rate, E (m kyr^{-1})	[2]$f_{bedrock}$	D_{50} (cm)	Number of Grains Measured	[3]$D_{50\ Fracture}$ (cm)	Bedrock Fracture Area Surveyed (m^2)
SG1602	28	34.1621	-117.6376	1.28 ± 0.19	0.33*	9±1	105	75	9,325
NSJM SG07-06*	13	34.2046	-118.0924	0.57 ± 0.11	0.14	22±4	674	x	0
SG08-09*	18	34.3692	-117.8394	0.37 ± 0.04	0.06	8±0.7	586	x	0
SJ0806	28	33.8738	-116.6796	0.151 ± 0.012	0.21*	45±4	635	325	25,887
SJ0807	11	33.8751	-116.6732	0.086 ± 0.008	0.27*	60±13	175	304	46,938
SJ1703	9.8	33.8397	-116.6137	0.53 ± 0.07	0.58*	29±8	119	239	2,388
Headwater catchments	**Drainage area (km^2)**	**Outlet Latitude (°)**	**Outlet Longitude (°)**	**Erosion rate, E (m kyr^{-1})**	**[2]$f_{bedrock}$**	**$D_{50\ channel}$ (cm)**	**Number of Grains Measured**	**[3]$D_{50\ Fracture}$ (cm)**	**Bedrock Fracture Area Surveyed (m^2)**
SG127	2.5	34.2187	-118.0855	0.68 ± 0.08	0.25	39±13	125	x	0
SG128	2.1	34.3381	-118.0106	0.036 ± 0.004	0.04	3±1	114	66	90
SGM SG131	2.2	34.3659	-117.9931	0.085 ± 0.013	0.01	0.8±0.2	102	46	78
SG132	2.2	34.3652	-117.99	0.093 ± 0.009	0.01	3±1	108	x	0
SG1601	1.2	34.1906	-117.6434	0.96 ± 0.16	0.23	30±4	377	x	0
SG1605	1.2	34.2036	-117.5867	2.2 ± 0.4	0.60	27±4	271	51	3,333
SG1608	4.3	34.214	-117.6075	0.63 ± 0.09	0.25*	23±2.3	559	69	4,592
SG1609	0.8	34.2226	-117.6076	0.60 ± 0.07	0.43	29±4	373	62	1,055
SG1703	1.3	34.2038	-117.6311	0.234 ± 0.024	0.25	27±2	1346	87	1,043
SG1705	1.9	34.2142	-117.6206	0.39 ± 0.05	0.41	33±1	2504	86	1,839
SG1706	1.2	34.2159	-117.5721	1.39 ± 0.19	0.68	29±3	541	89	567
SGB07	3.1	34.2979	-118.1487	0.22 ± 0.04	0.12	4±1	108	x	0
SJ0801 NSJM	6.5	33.8117	-116.6428	0.040 ± 0.003	0.13± 0.08**	0.5±0.1	161	x	0
SJ0804	5.4	33.7797	-116.646	0.044 ± 0.004	0.13	6±2	107	93	238
SJ0805	6.8	33.7765	-116.6485	0.061 ± 0.005	0.05	2.0±0.6	107	x	0
SJ1601	3.6	33.8329	-116.6589	0.154 ± 0.014	0.48	89±11	423	304	46,938
SJ1603	1.2	33.8296	-116.6784	0.202 ± 0.019	0.61	150±25	249	325	25,887
SJ1604	1.3	33.8357	-116.6997	0.16 ± 0.014	0.53	117±30	126	x	0
SJ1605	2.5	33.835	-116.7005	0.251 ± 0.023	0.28	114±13	461	x	0
SJ1701	0.7	33.8365	-116.6357	0.234 ± 0.023	0.41	86±5	1347	239	2,388
SJ1702	1.2	33.8298	-116.6354	0.61 ± 0.09	0.52	126±10	825	x	0

892 [1] All samples recorded in Neely et al., 2019 with exception of samples denoted by *, where erosion rates are calculated from ^{10}Be concentrations
893 reported in DiBiase et al. (2010) and Heimsath et al. (2012) as recalculated by Neely et al. (2019). Lat, Long, and drainage area refer to
894 downstream-most location of grain size surveys associated with each ^{10}Be-derived erosion rate.
895 [2] The fraction of bare bedrock exposed on hillslopes, $f_{bedrock}$, are reported in Neely et al., 2019 with exception of samples denoted by *, where
896 $f_{bedrock}$ is estimated from linear regression between mean hillslope angle and $f_{bedrock}$ (Neely et al., 2019), and **, where $f_{bedrock}$ is determined from
897 mapping with 0.5-m resolution imagery from ArcGIS 10.2 world-imagery (DigitalGlobe, 2014, 2017).
898 [3] "x" denotes that bedrock fracture spacing was not quantified on any cliffs within watershed, typically due to inaccessibility or extensive soil-
899 cover and no available bedrock cliff structure-from-motion models (Fig. 1)
900
901

902 **Table 2.** Parameters used for sediment grain size fining model (Eq. 1; Fig.11)

Landscape	h (m)[1]	α (kyr m^{-1})[2]	k_1 [3]	k_2 (m kyr^{-1}) [3]	k_3 [3]	E_{crit} (m kyr^{-1}) [2]	D_{50} fracture (cm) [4]	D_{50} min (cm) [1]
NSJM	1	2.27	0.4	0.050	0.4	0.08	299	0.01
SGM	1	0.51	0.5	0.025	0.5	0.2	63	0.01

903 [1] Parameter value estimated from field observations and held constant.
904 [2] Parameter derived using linear regression between catchment averaged erosion rate and bare-bedrock hillslope abundance from
905 Neely et al., (2019)
906 [3] Calculated by minimizing sum-squared-residual (SSR) between modeled D_{50} grain sizes and measured D_{50} grain sizes as a
907 function of increasing catchment averaged erosion rate (Fig. 11 B-C).
908 [4] Parameter value derived from field measurements (Fig. 9 C-D).
909
910
911
912
913
914
915
916

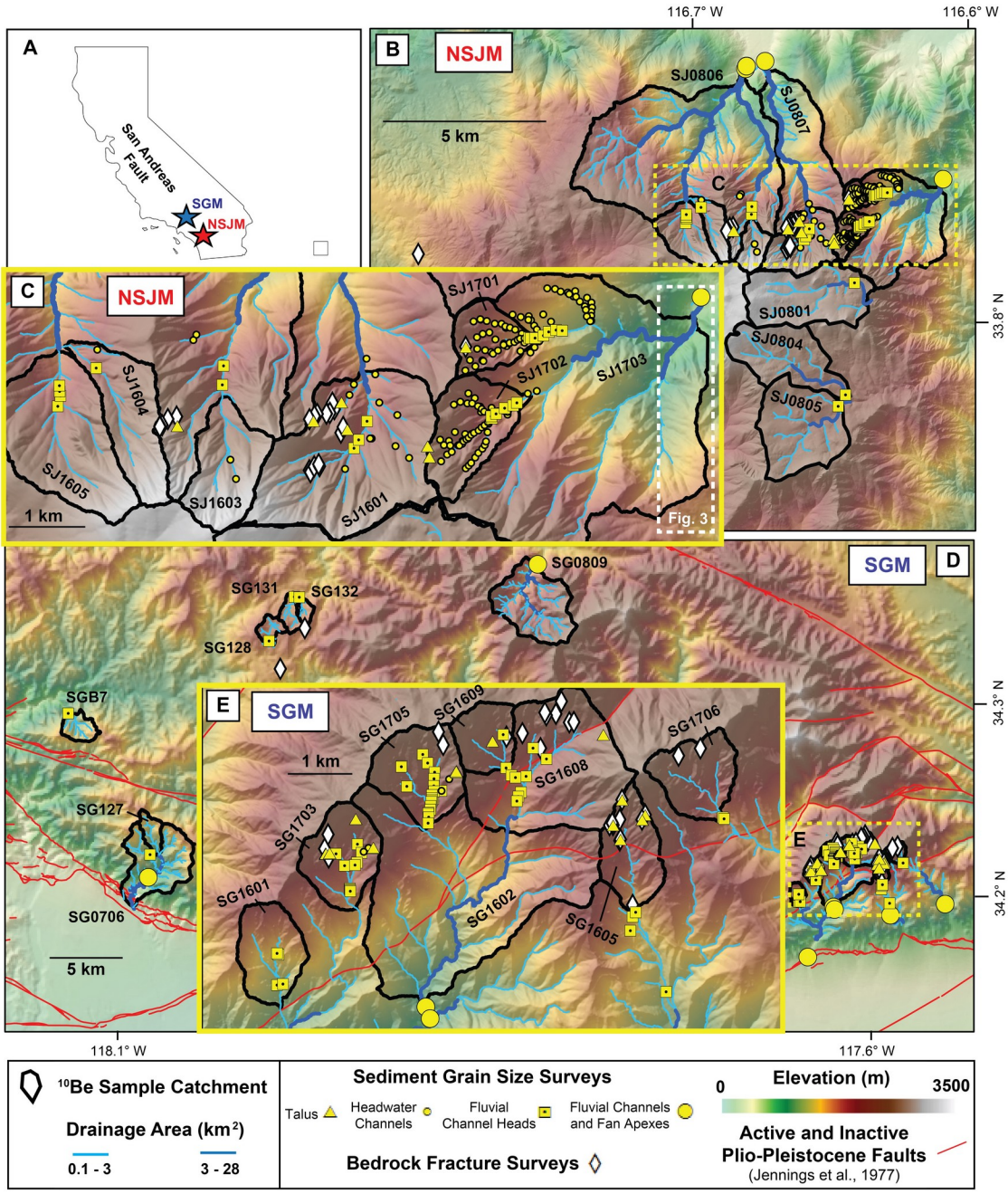

Figure 1. (A) Location of northern San Jacinto Mountains (NSJM) and San Gabriel Mountains (SGM) in southern California, USA. (B-E) Location of sediment grain size and bedrock fracture spacing surveys within ^{10}Be sample catchments in NSJM (B-C) and SGM (D-E), classified by landscape position. Inset maps show catchments with high-data density in (C) NSJM and (E) eastern SGM. White-dashed box in (C) is the location of longitudinal profile in Fig. 3.

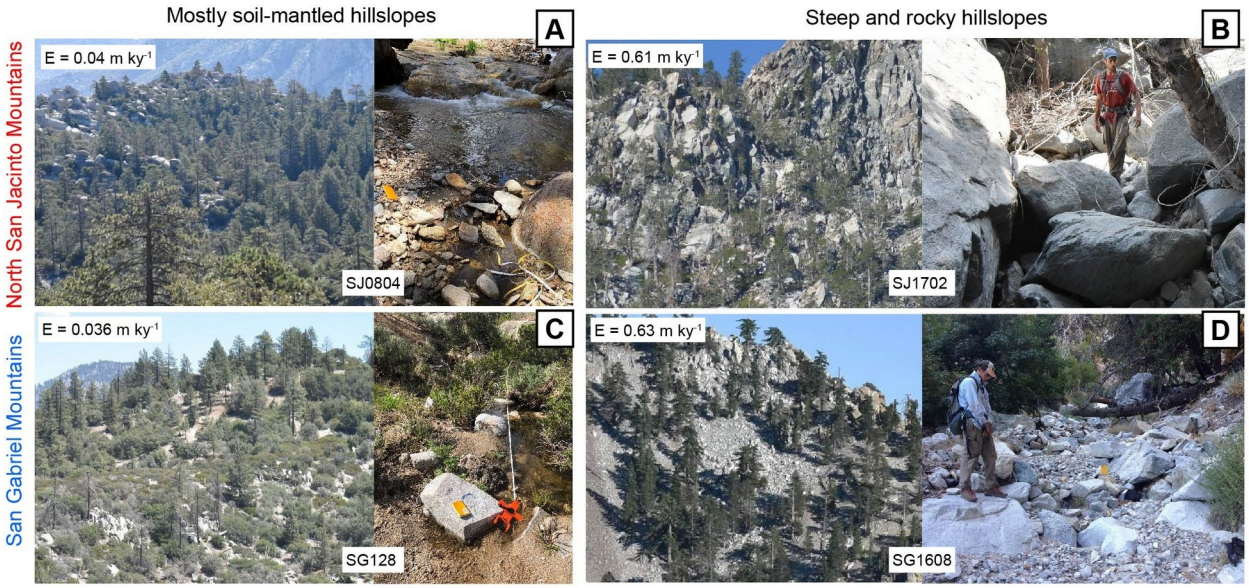

Figure 2. Example hillslopes and channel bed material from the northern San Jacinto Mountains (A, B) and San Gabriel Mountains (C, D) in soil mantled catchments (A, C) and steep catchments with bedrock cliffs (B, D). "E" indicates erosion rate determined from in situ ^{10}Be concentrations in stream sediment (DiBiase et al., 2010; Rossi, 2014; Neely et al., 2019). Scale is approximately the same for hillslope photographs and for channel bed photographs.

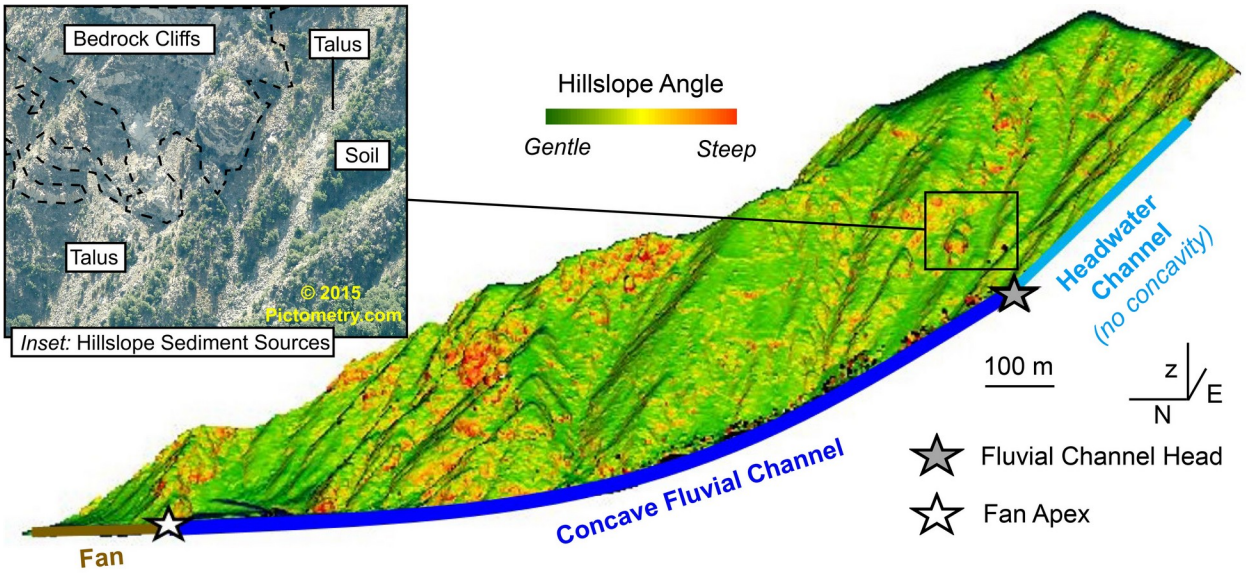

Figure 3. Example longitudinal profile (blue) along the trunk stream of a steep, rocky catchment (SJ1703) with background hillslopes and headwater channels shaded by local gradient. Annotations highlight geomorphic process domains distinguished throughout this manuscript (section 2.2). Inset shows oblique air photo of hillslope sediment source types over the extent of the outlined black rectangle.

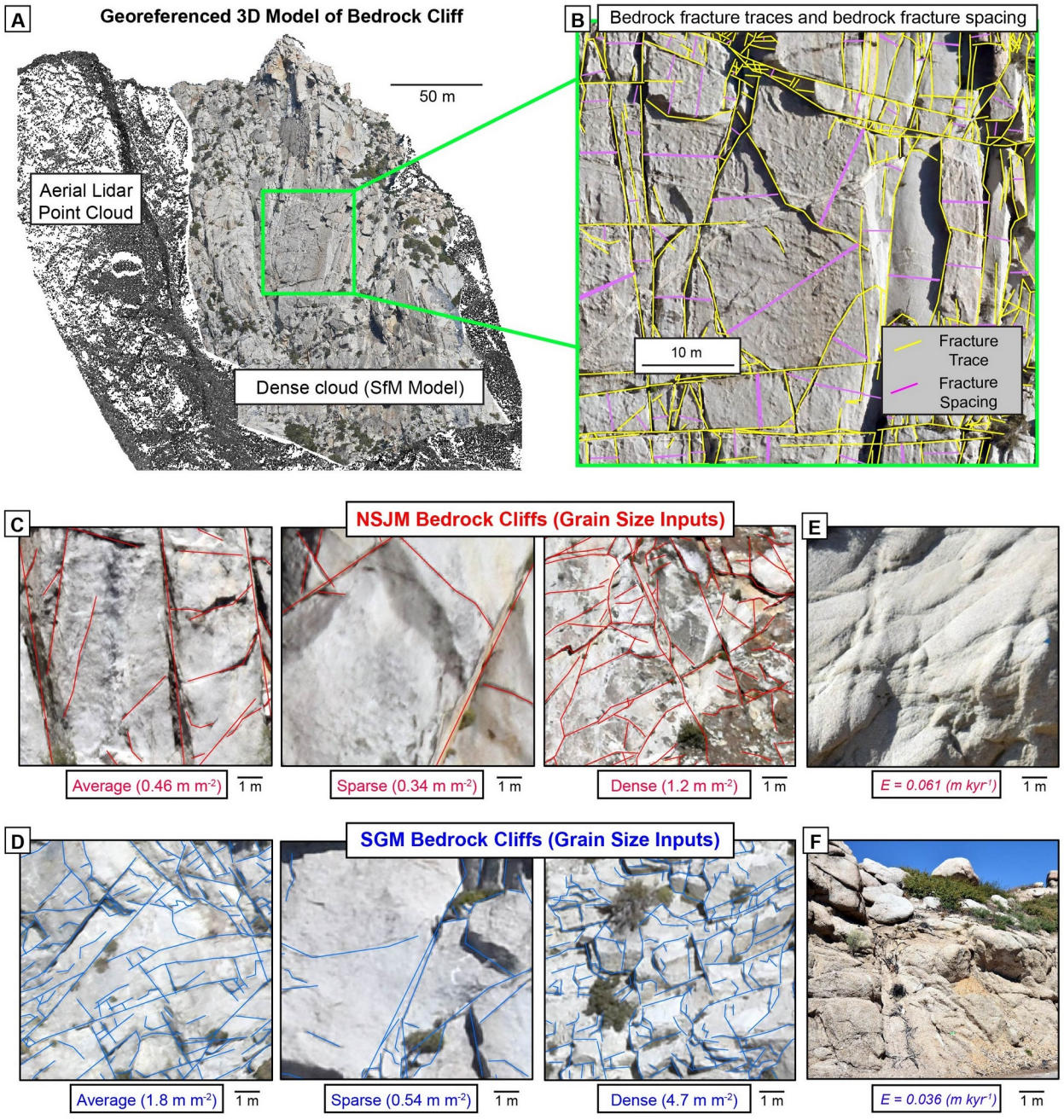

Figure 4 (A) Cliff SJ1603-2 shown with structure-from-motion photogrammetry (SfM) point cloud (colorized points) aligned to the airborne lidar point cloud (black points). (B) 1-cm resolution orthophoto extracted from region within green box. Yellow lines are bedrock fracture traces used to calculate fracture density. Pink lines show bedrock fracture spacing between fracture traces. (C-D) Orthophotos showing fracture traces and the range of bedrock fracture densities for cliffs from the northern San Jacinto Mountains (NSJM) (C) and San Gabriel Mountains (SGM) (D). (E-F) Field photographs show weathered bedrock in road cuts from soil-mantled catchments in the (E) NSJM and (F) SGM.

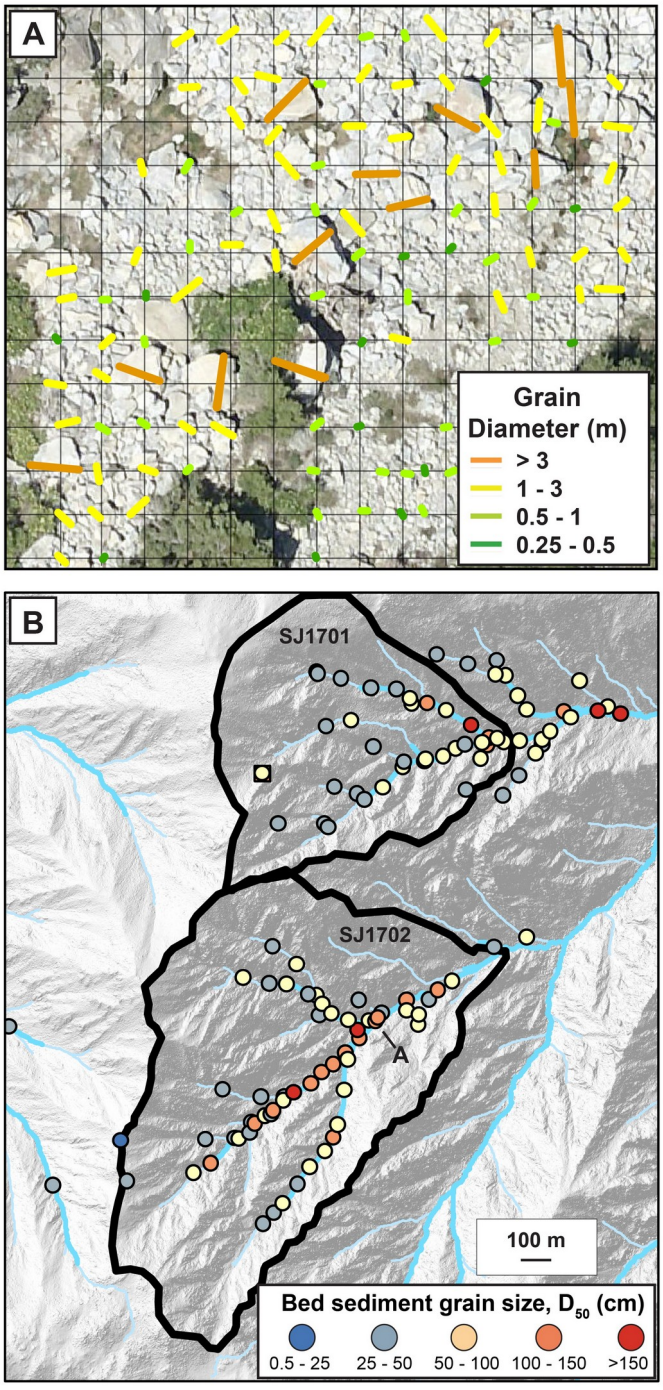

Figure 5. (A) Example orthophoto overlain by a 4-m grid shows individual grain diameter measurements from Chino Canyon in NSJM (catchment SJ1702, location shown in panel B). Grain-diameter measurements are not shown for grains with diameters smaller than 0.25 m. (B) Continuous grain diameter measurements made throughout catchments SJ1701 and SJ1702 in NSJM are discretized into individual grain size surveys (colored circles). Blue lines denote channel network with drainage area >0.025 km^2 and black polygons outline watersheds upstream from ^{10}Be sample locations.

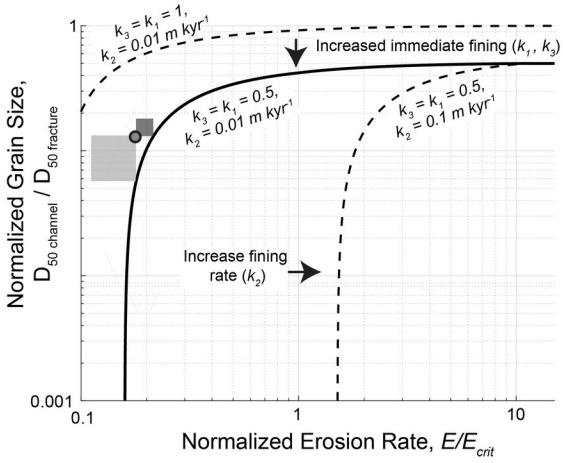

Figure 6: Predicted relationship between normalized grain size and normalized erosion rate from hillslope sediment fining model (Eq. 1). Dashed curves illustrate model sensitivity to parameters k_1, k_2, and k_3, assuming same initial fining for soil-mantled and bedrock hillslopes ($k_1 = k_3$). Example data point (grey circle) shows example calculation of squared residuals in normalized erosion rate (light grey square) and normalized D_{50} grain size (dark grey square) directions (Eq. 4b). For each field-data point, the minimum of these two residuals was used to calculate sum-squares residuals (Eq. 4a) and fit k_1, k_2, and k_3 values to field data (Fig. 11B-C).

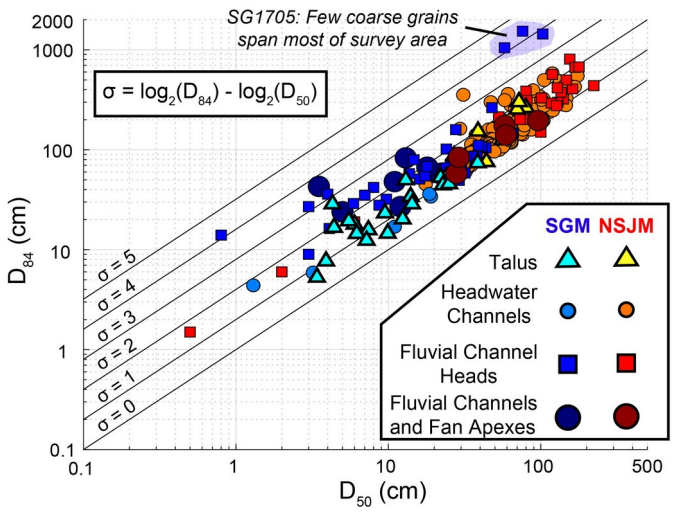

966

967 **Figure 7:** Plot of D_{84} versus D_{50} for all sediment grain size distributions highlighting similar
968 range of sorting coefficient, σ, for all sample types and for both landscapes. Large D_{84} values
969 from surveys highlighted in blue result from few coarse grains spanning ~20% of the individual
970 survey area.
971

972

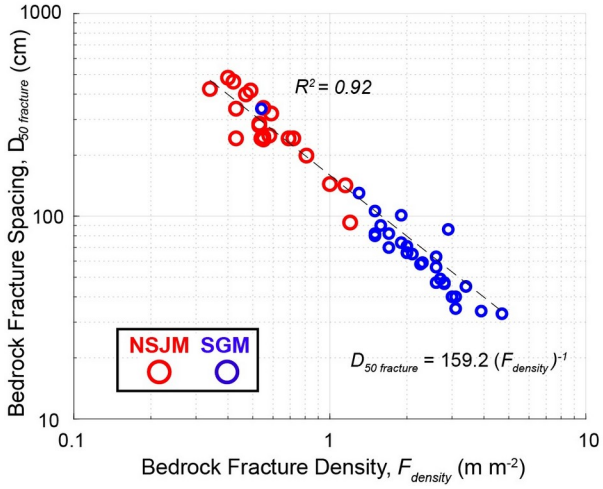

973

974 **Figure 8.** Median bedrock fracture spacing, $D_{50\ fracture}$, plotted against bedrock fracture density,
975 $F_{density}$, measured for each cliff in the northern San Jacinto Mountains (NSJM; N = 21) and San
976 Gabriel Mountains (SGM; N = 29).
977
978
979
980
981
982
983
984
985
986
987

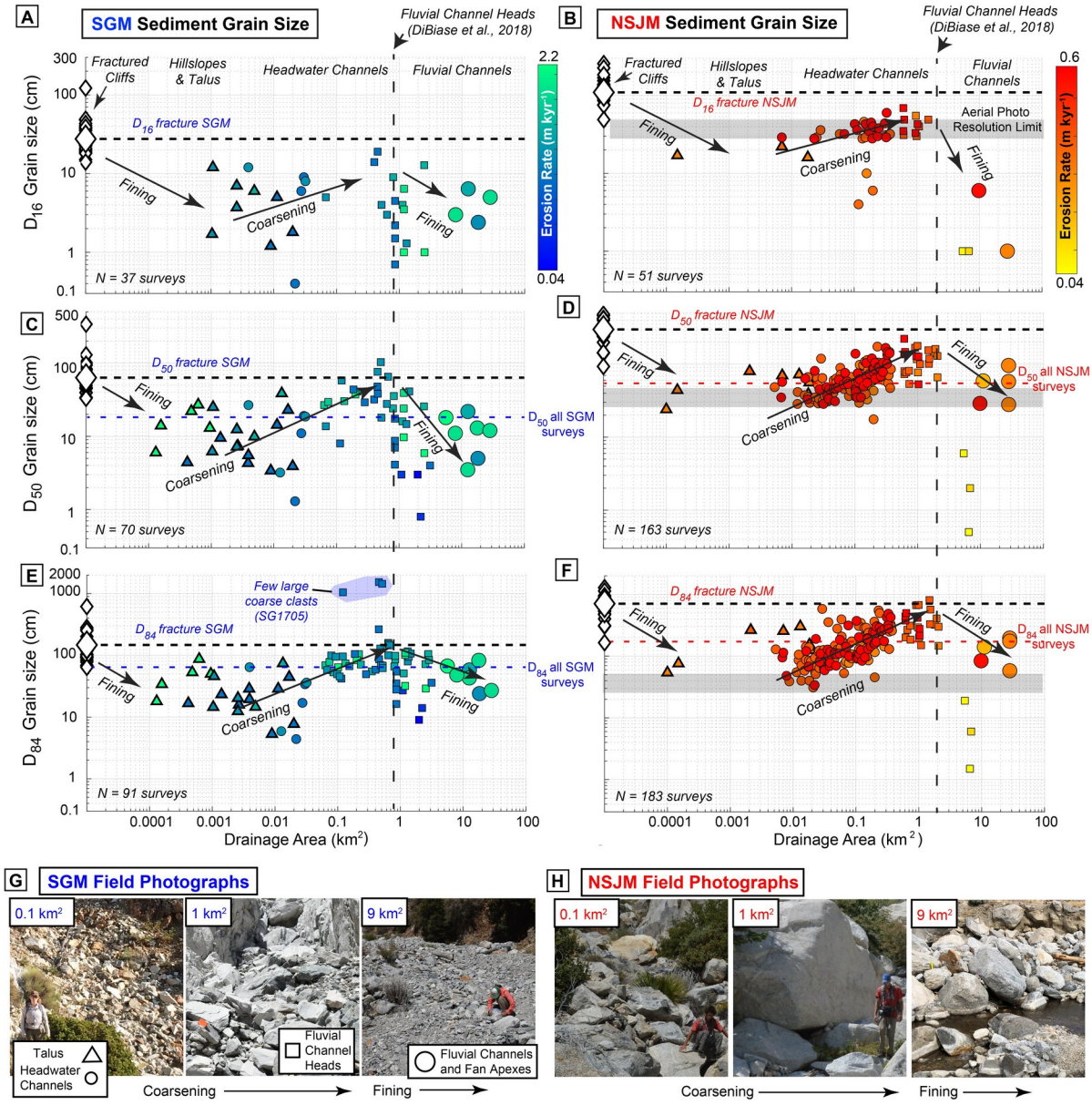
A
SGM Sediment Grain Size
Fluvial Channel Heads (DiBiase et al., 2018)
Fractured Cliffs
Hillslopes & Talus
Headwater Channels
Fluvial Channels
D16 Grain size (cm)
D16 fracture SGM
Fining
Coarsening
Fining
N = 37 surveys
Erosion Rate (m kyr-1)
2.2
0.04
B
NSJM Sediment Grain Size
Fluvial Channel Heads (DiBiase et al., 2018)
Fractured Cliffs
Hillslopes & Talus
Headwater Channels
Fluvial Channels
D16 fracture NSJM
Aerial Photo Resolution Limit
Fining
Coarsening
Fining
N = 51 surveys
Erosion Rate (m kyr-1)
0.6
0.04
C
D50 Grain size (cm)
D50 fracture SGM
Fining
Coarsening
Fining
D50 all SGM surveys
N = 70 surveys
D
D50 fracture NSJM
Fining
Coarsening
Fining
D50 all NSJM surveys
N = 163 surveys
E
D84 Grain size (cm)
Few large coarse clasts (SG1705)
D84 fracture SGM
Fining
Coarsening
Fining
D84 all SGM surveys
N = 91 surveys
Drainage Area (km2)
F
D84 fracture NSJM
Fining
Coarsening
Fining
D84 all NSJM surveys
N = 183 surveys
Drainage Area (km2)
G
SGM Field Photographs
0.1 km2
1 km2
9 km2
Talus
Headwater Channels
Fluvial Channel Heads
Fluvial Channels and Fan Apexes
Coarsening
Fining
H
NSJM Field Photographs
0.1 km2
1 km2
9 km2
Coarsening
Fining

988

989 **Figure 9.** Downslope and downstream trends in sediment grain size for the San Gabriel
990 Mountains (SGM, left panels) and northern San Jacinto Mountains (NSJM, right panels). The
991 grain size fractions D_{16} (A-B), D_{50} (C-D), and D_{84} (E-F) are shown plotted against upstream
992 drainage area. Fracture spacing measured on bedrock cliffs is marked on the y-axis of each panel
993 by white diamonds, with large white diamond and black dashed line representing the D_{16} (A-B),
994 D_{50} (C-D), and D_{84} (E-F) of summed fracture spacing distribution from all cliffs in each
995 landscape. The D_{50} and D_{84} from all channel surveys is marked in both landscapes with a colored
996 horizontal line. Symbol color and symbol shape correspond to catchment averaged erosion rate
997 and geomorphic-process-domain associated with each grain size survey (see panel G for symbol
998 key). Aerial photograph resolution limit (28–48 cm) is marked on NSJM plots. The number of
999 surveys with resolvable D_{16}, D_{50}, or D_{84}, *N*, is marked in bottom left corner of panels A-F. (G-H)
1000 Field photographs of sediment grain size at increasing drainage areas. All photographs have
1001 approximately the same scale.

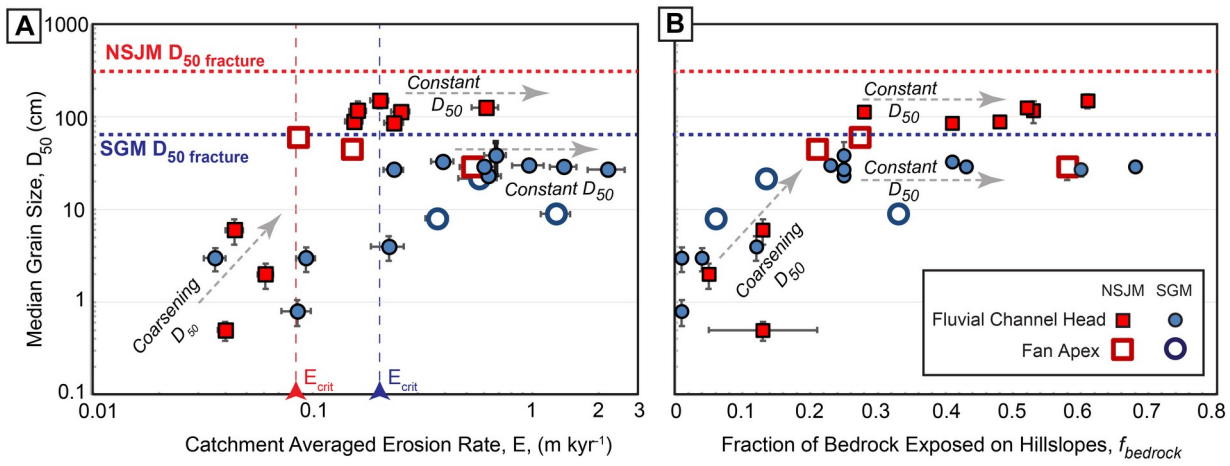

Figure 10: Trends in median fluvial grain size, D_{50}, as a function of (A) increasing catchment erosion rate and (B) bare-bedrock hillslope abundance in the northern San Jacinto Mountains (NSJM, red) and San Gabriel Mountains (SGM, blue). Vertical dashed lines show catchment erosion rate E_{crit}, above which bedrock hillslope abundance increases systematically (Neely et al., 2019). Fluvial channel head data reflect sample catchments with drainage areas ranging from 0.5–7 km^2 in the NSJM and 0.05–3 km^2 in the SGM. Fan apex data indicate measurements from active channels with drainage areas larger than 7 km^2.

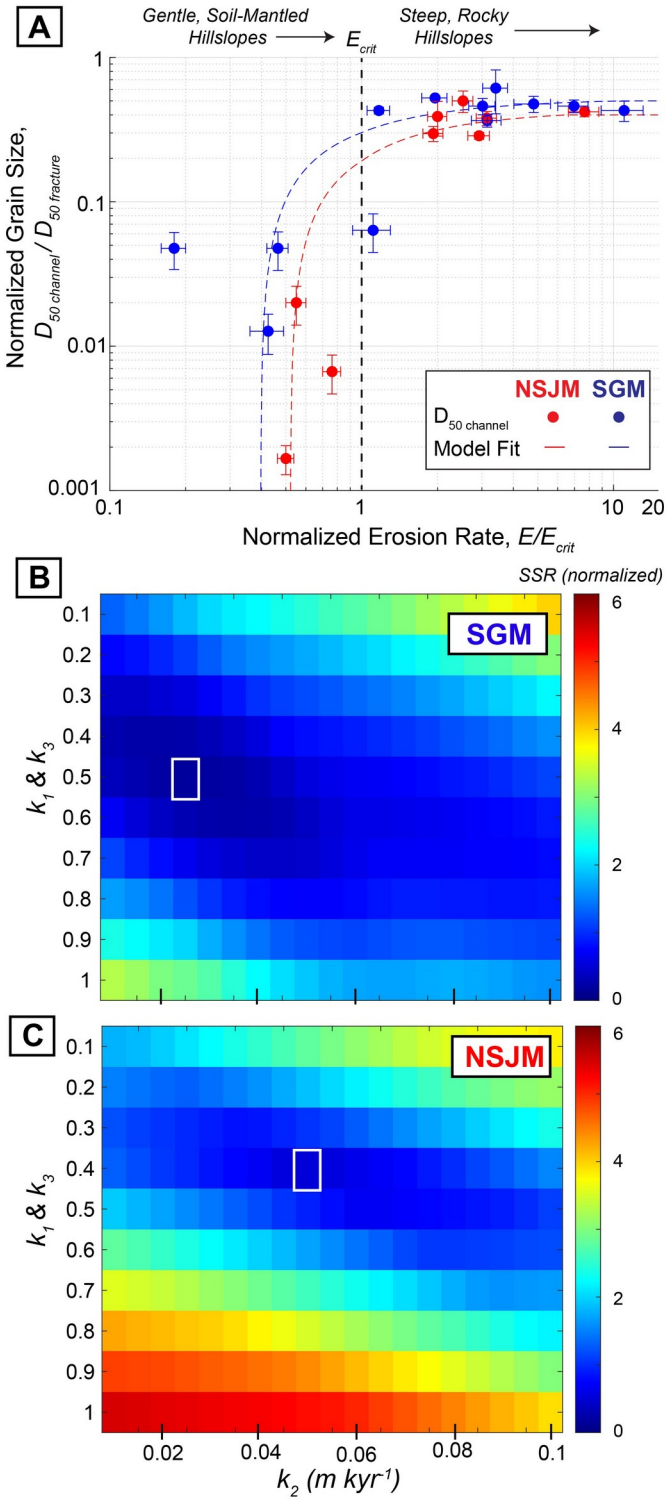
A
Gentle, Soil-Mantled Hillslopes
E_{crit}
Steep, Rocky Hillslopes
Normalized Grain Size, $D_{50\ channel} / D_{50\ fracture}$
Normalized Erosion Rate, E/E_{crit}
NSJM SGM
$D_{50\ channel}$
Model Fit
B
SSR (normalized)
SGM
k_1 & k_3
C
NSJM
k_2 ($m\ kyr^{-1}$)

1011

Figure 11. (A) Comparison between modeled sediment grain size delivered from hillslopes and measured sediment grain size at fluvial channel heads. E_{crit} is erosion rate above which bedrock exposure on hillslopes systematically increases. Vertical error bars result from bootstrap analysis and error values reported in Table 1, and parameter values used are listed in Table 2. (B-C) Plot of the sensitivity of the sum of the squared residuals, SSR, to variation in the model fining parameters k_1=k_3 and k_2 (Equation 4). Model results in (A) shown for best-fit parameter combination for SGM (B) and NSJM (C), which are highlighted with a white box in (B) and (C).

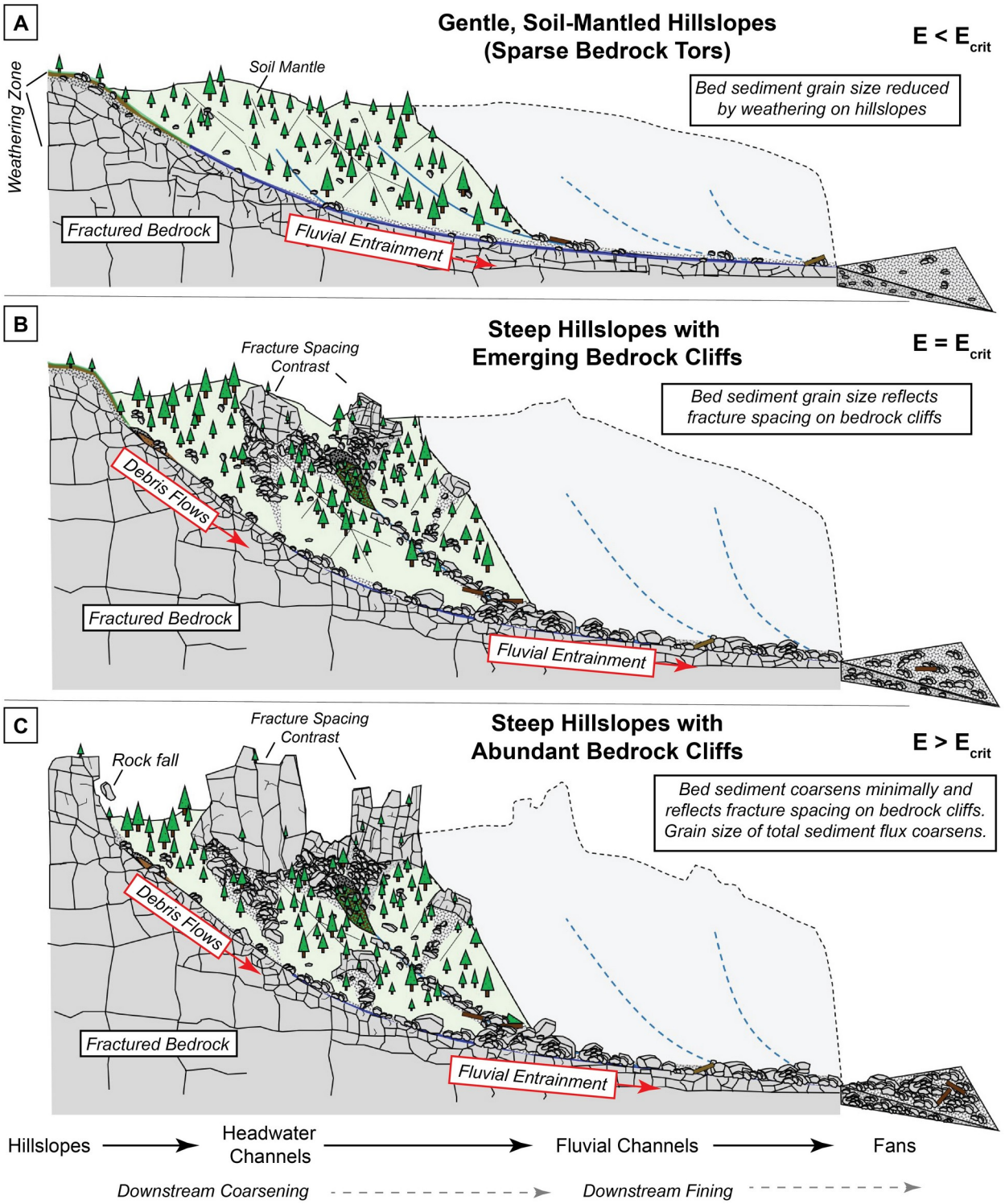

Figure 12. Conceptual model showing landscape-scale grain size patterns as a function of increasing catchment erosion rate, E, and bare-bedrock hillslope abundance, $f_{bedrock}$.